<div align="center">**Reply to reviewers**</div>

<div align="center">**acp-2015-902**</div>

<div align="center">**Detection of Saharan dust and biomass burning events using near real-time intensive aerosol optical properties in the northwestern Mediterranean.**</div>

The authors would like to thank the reviewer for their comments and suggestions, which helped improving the quality of this work. A new version of the manuscript has been prepared following the suggestions. We provide below detailed replies to each of the comments.

Anonymous referee #1

<u>Reviewer#1. General comment 1)</u>. **This paper by Ealo et al. presents a very interesting idea for the real-time detection of dust and biomass burning events. However, one major concern I see with this technique is the difficulty to differentiate between the dust and biomass burning events, both dust and biomass being strong absorber in UV. This issue might be bigger in summer when the co-occurrence of SDE and Wildfire events may be highly probable. Due to re-circulation, these events may not be differentiated over prolonged time scales. Please discuss.**

<u>Reply to Reviewer#1. General comment 1)</u>. The authors agree with the referee that the concomitance of biomass burning and wildfires episodes during Saharan dust events (SDE) may be an issue. As stated in the manuscript, one of the objectives of this paper is to study the limitations of the proposed technique, firstly developed by Collaud Cohen et al. (2004), and to highlight the necessity of a better estimation of the different episodes through a multidisciplinary approach.

For example, as we show in the manuscript, wildfires events can be detected by means of different tools such as back-trajectories, forecast models and remote sensing data (satellite images, ceilometer/LIDAR and sun photometers measurements), and considered as isolated events (Fig. 8 in the manuscript). Concerning biomass burning events, the scattering Ångström exponent (SAE) parameter is certainly a useful parameter to establish differences between mineral dust (coarse material) and biomass burning (finer aerosol). Moreover, it is also possible to consider online PMx mass data in order to assess the SAE parameter regarding the changes in the size of aerosols. In addition, the black carbon concentration, which considerably increases during biomass burning events (See Fig. 8 describing a wildfire episode in the manuscript), can be also investigated. Furthermore, offline chemical filter analysis is a valuable input for the identification of iron oxides contained within the mineral dust to characterize the atmospheric situation.

It should be also considered that biomass burning is an active source in winter in the area under study and that during the study period (2012-2014) only three SDE were identified in winter. Furthermore, biomass burning concentration is relatively lower compared to northern areas in Europe; annual average contribution was estimated in 36%. During these winter SDE we did not see a marked daily cycle of AAE, therefore the dominance of mineral dust appears to be larger with respect to biomass burning regarding the effects on intensive optical properties.

In order to take into account the Referee's comment the following sentence has been added to section 5.3.3 in the revised manuscript:

"The concomitance of biomass burning and wildfire episodes during SDE may be an issue, being both dust and biomass burning strong absorbers in the UV. The SAE is a useful parameter that should be considered in order to establish differences in near real-time between mineral dust (coarse material) and biomass burning (finer aerosol). However, since relatively low biomass burning concentration was found in the area under study, the dominance of mineral dust appears to be larger with respect to biomass burning regarding the effects on intensive optical properties. Furthermore the co-occurrence of SDE and biomass burning winter emissions is not usual. Whereas for differentiating wildfires and SDE, both frequently occurring during summer, wildfires events can be considered as isolated events and detected by means of different tools such as back-trajectories, forecast models and remote sensing data".

Reviewer#1. General comment 2). This technique makes use of intrinsic properties of the aerosol species like Absorption, Scattering and Single Scattering Albedo Angstrom Exponents. However, these properties are influenced by environmental factors like temperature, RH, aerosol aging time, which is not discussed in this study. A part of difference in aerosol optical properties between MSY and MSA may be due to the fact that aerosol processing at these locations may be different and aerosol may have different properties. These concerns are highlighted especially during the re-circulation events. Please discuss.

Reply to Reviewer#1. General comment 2). The most important ambient parameter affecting scattering measurements is RH. High values of RH produce hygroscopic growth on particles, enhancing the scattering coefficient. It should be note that nephelometer measurements were made at constant RH, lower than 40%, following standards recommended by ACTRIS in order to avoid possible scattering enhancement due to hygroscopicity. Moreover, also the temperature (changing with RH) is controlled in the nephelometer cell and kept at almost constant values throughout the year.

Certainly, the aging of the aerosols affects the aerosol intensive optical properties (IOP). However, the study of aerosol aging is far beyond the scope of this work. In this manuscript we are mainly interested in studying how IOP change during SDE and biomass burning events, which dominate the IOP during their occurrence. Moreover, as we show in the manuscript, the proximity to anthropogenic sources of fine PM is the main affecting the SSAAE.

Despite this fact, the effect of aerosol aging time on the intensive optical properties is partially considered and discussed in the text within the air mass origin analysis, where Atlantic advections, Saharan dust events and re-circulation episodes were considered (Fig. 2a and 2d in the manuscript). Atlantic advections, occurring more frequently during winter, are characterized by dominance of fresh aerosols. MSA is usually within free troposphere during the colder period and influenced by clean air masses from Atlantic advections. However re-circulation episodes usually take place during warmer months, when both stations are frequently within the planetary boundary layer. These episodes are identified by stagnated air masses, high insolation and lack of precipitation lasting for few days, resulting in a dominance of aged aerosol. Probably the aerosol aging time is more pronounced at MSA, since it is more isolated from fresh anthropogenic pollutant sources transported mainly from Barcelona urban and industrial areas. Then pollutants at MSA present larger atmospheric residence time and thus also probably stronger aging process than at MSY.

Nevertheless, for a deeper evaluation of how these variables independently affect the intensive optical properties it would be necessary to perform specific studies, such as evaluating the aerosol aging time and coating processes.

Reviewer#1. Specific comment 1). The nephelometer instrument was calibrated only 3 times a year and zero adjust was carried out once a day may possibly insufficient for unbiased measurements. Some plots or data showing the stability of the instrument can be helpful in supporting the frequency of calibration and zero adjustments.

<u>Reply to Reviewer#1. Specific comment 1)</u>. We calibrated both nephelometers following the standards proposed by ACTRIS network in order to obtain high quality data, and comparability among all ACTRIS stations. Both instruments have participated in workshop intercomparisons organized by ACTRIS and showed satisfactory comparability with other EU nephelometer and "reference" instruments.

As an example, Figure 1 shows the stability of nephelometer measurements at MSA station. Figure 1 shows the average scattering coefficients at the three wavelengths for different percentiles (0.05, 0.25, 0.50, 0.75, 0.95) during zero check calibration for the year 2013. Average ± standard deviation are reported for each wavelength during zero check. Since acceptable limits for zero check are set in ±2 Mm^{-1}, our data are within the standards recommended by the manufacturer.

It should be noted that some problems concerning the stability of measurements were found after long-distance transportation. However, most of these problems were solved through a full calibration of the nephelometer.
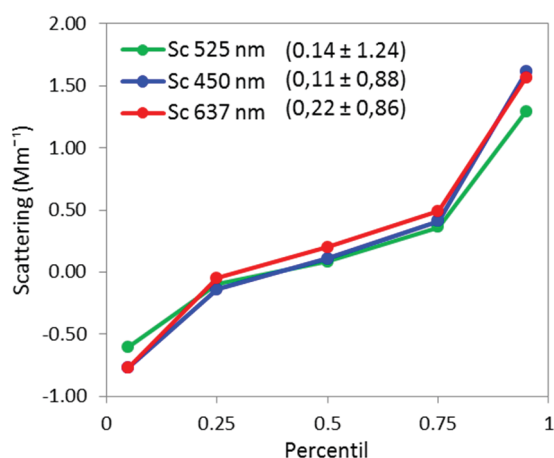

Figure 1. Average scattering coefficients for the calculated percentiles (0.05, 0.25, 0.50, 0.75, 0.95) during zero check calibration measurements at 450, 525 and 635 nm for the year 2013 at MSA station. Average and standard deviation of scattering for the three wavelengths during the whole period are also reported.

<u>Reviewer#1. Specific comment 2)</u>. In order to help the reader, please provide average and standard deviation values in parentheses while comparing the optical properties in different events or between the two stations.

<u>Reply to Reviewer#1. Specific comment 2)</u>. We agree with the Referee that this information is missing in the manuscript. It should be considered, however, that data within the Ångström matrix are displayed on hourly base whereas air mass origin was identified once per day, therefore average values during a whole day could include some hourly data points which are not representing these situations. Nevertheless, ranges of SAE, AAE and %PM$_{1-10}$ for different air mass origin provided in the text are meaningful in order to consider limit values purely representing these atmospheric situations.

In order to consider the Referee's comment, the frequency distribution plots of SAE and AAE for SDE, regional episodes (REG) and Atlantic advections (ATL) will be added in the supporting material (Fig. 2a and 2b for MSY and MSA). These plots will help the reader to interpret the variability of the intensive properties and establish differences among atmospheric scenarios at both stations.

Accordingly to the referee's suggestion, the following sentence was added to section 5.2 of the Manuscript: "Further information providing the frequency distribution and average value of SAE and AAE for each atmospheric scenario is reported in Figs. S1a and S1b for MSY and MSA.
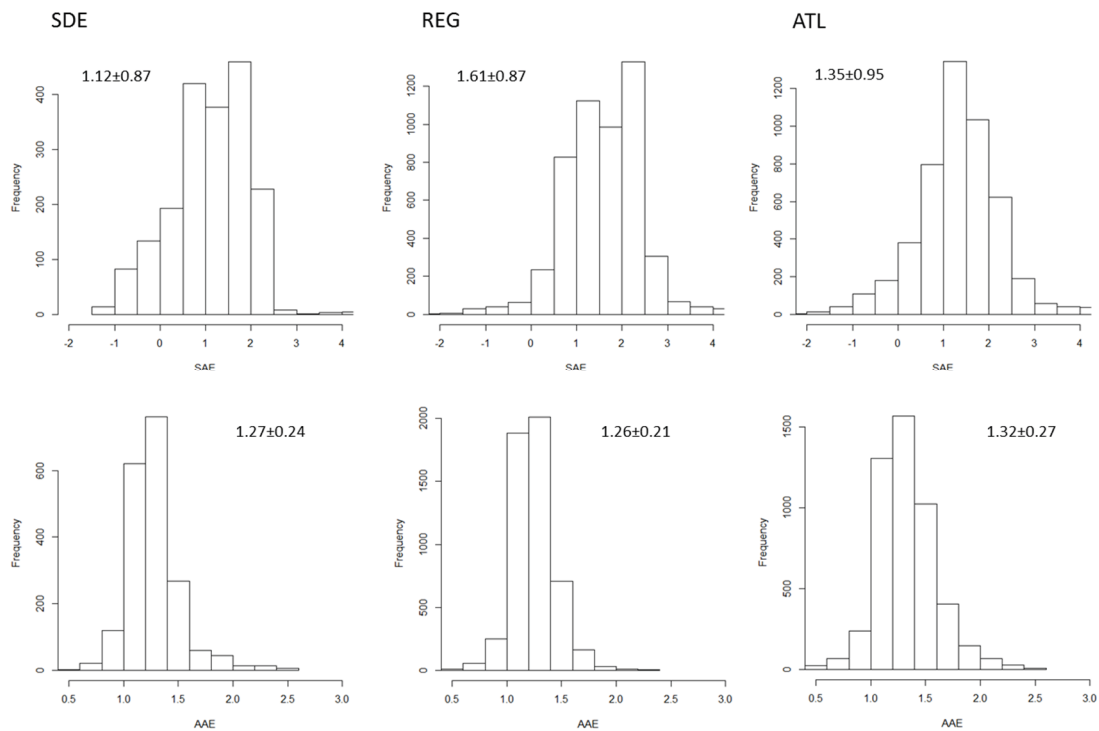
Figure 2a. Frequency distribution of SAE and AAE parameters for the three atmospheric scenarios (SDE REG, ATL) displayed in the Ångström matrix at MSY. Average and standard deviation of these parameters are also reported for the whole period (2012-2014).
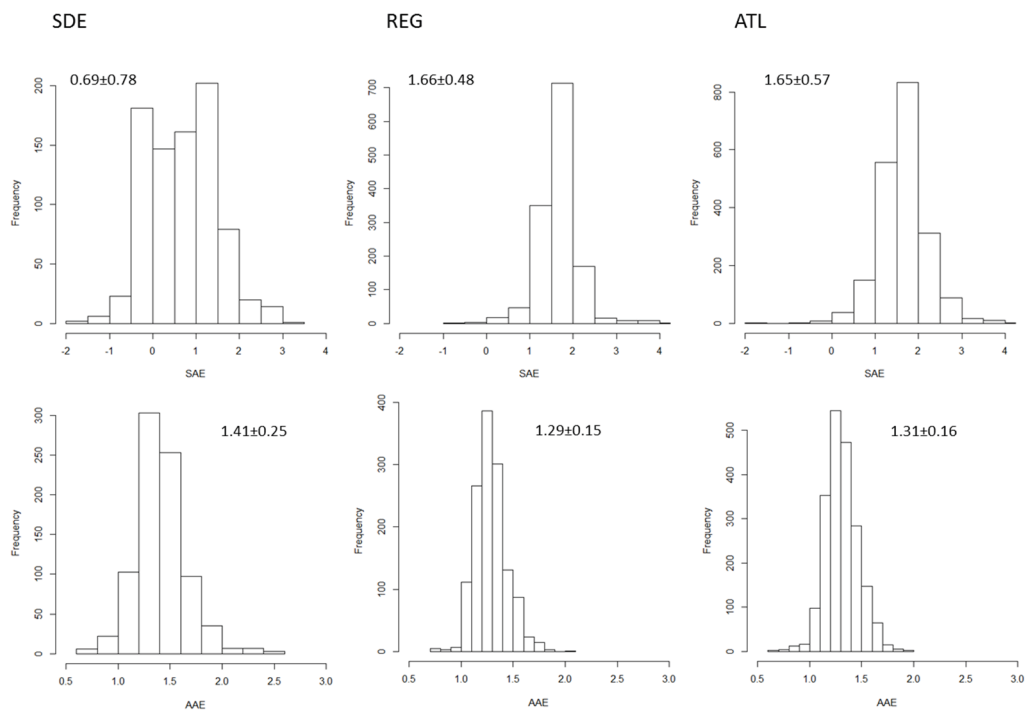
Figure 2b. Frequency distribution of SAE and AAE parameters for the three atmospheric scenarios (SDE, REG, ATL) displayed in the Ångström matrix at MSA. Average and standard deviation of these parameters are also reported for the whole period (2013-2014).

Reviewer#1. Specific comment 3). Line 511: "bellow" correction: below.

Reply to Reviewer#1. Specific comment 3). It has been corrected.

Reviewer#1. Specific comment 4). Lines 592 and 593: please provide the abbreviated station names in the heading.

Reply to Reviewer#1. Specific comment 4). It has been corrected.

Reviewer#1. Specific comment 5). Lines 553- Lines 560: Thee fraction of BBOA and HOA in previous studies may be dependent upon the time of the year those measurements were made. So how fair it is to make those assumptions based on the observations in previous study?

Reply to Reviewer#1. Specific comment 5). Effectively, it is not far enough to consider the POA to SOA ratios from previous studies carried out during not identical periods of the year. Unfortunately, as stated in the manuscript, we did not performed any experiment, simultaneously to the study period, for differentiating primary from secondary organic sources (such as using levoglucosan as biomass burning tracer), and then we had to resort to results obtained in previous studies since it is the unique information we have to establish POA to SOA relations. In order to differentiate primary from secondary OM_{bb}, we considered the proportion of SOA originated from BBOA reported by Cubison et al. (2011). This ratio was primary applied to the results of the source apportionment to ACSM performed at MSY station (Minguillón et al., 2015), which were also used in this study. For OM_{ff}/HOA ratio, we considered results from previous studies performed also at MSY using ^{14}C technique (Minguillón et al., 2009).
Thus, we do not have the necessary information to evaluate how much the use of non-simultaneous ancillary data is affecting our results. However, even though these assumptions concerning POA to SOA ratios are not from measurements carried out in the same study, the considered results for AAE_{ff} and AAE_{bb} (1 and 2 respectively) satisfactory agreed with those coefficients used in previous studies deploying the Aethalometer model.

Following the referee 's suggestion section 5.3.2 in the revised manuscript has been modified as follows:

"Since simultaneous experimental data to the study period were not deployed for differentiating POA to SOA ratios, we have considered results previously reported for MSY measurements. SOA formation from biomass burning emissions can be up to 25% of the BBOA emitted, as shown by Cubison et al. (2011) using Aerosol Mass Spectrometer (HR-ToF-AMS) data. This ratio was primarily applied by Minguillón et al. (2015) to the results obtained from the source apportionment to ACSM performed at MSY station, which were also used in this study."

Reviewer#1. Specific comment 6). Lines 651 and 678: "leaded" correction: lead

Reply to Reviewer#1. Specific comment 6). It has been corrected as "led" instead of "lead".

Reviewer#1. Specific comment 7). Supplementary tables S1 should be numbered S1 (a) and S1 (b) as they are discussed in the text.

Reply to Reviewer#1. Specific comment 7). It has been corrected.

Anonymous referee #3

<u>Reviewer#3. General comment 1).</u> **The present paper propose to investigate the potential of detection of Saharan dust and biomass burning events at surface stations. The proposed set-up is based on optical measurements (scattering and absorption) made with multi wavelength nephelometer and aethalometer. More specifically the idea is to use the wavelength dependence of scattering and absorption of the aerosol as a function of their composition (i.e of their sources). The topic of the paper is really very interesting since the possibility of distinguishing the aerosol source and composition is a big challenge for air quality control also in relation with climate change. Moreover it can participate to improve our skills to exploit the data available at supersites that have been set-up in the last decade over Europe in the framework of infrastructure programs like ACTRIS. For these reasons, I think that this paper deserve to be published in ACP journal but some minor corrections and improvement are mandatory before publication.**

In general, i believe that a clear statement/summary about the possibility of detecting SDE and BB events is missing. What are the good conditions in which you can detect SDE event at the end? I have the impression that only almost "pure" SDE event are detectable and it is possible only at altitude/remote site. What is the best indicator to do that finally? I am not convince by SAE (a lot of overlap in scatter plots) and more by SSAAE.

<u>Reply to Reviewer#3. General comment 1).</u>

As we discussed throughout the article, detection of SDE by using the intensive optical properties are dependent on the degree of background pollution and the intensity of the event, since the effect of mineral dust on wavelength dependence may be hindered by anthropogenic pollutants. Thus, the intensive properties have to be calibrated for each sampling site, in order to better characterize the atmospheric aerosols.

Nevertheless, optical instruments, such as nephelometer and aethalometer, are widely used within monitoring networks such as ACTRIS and present several advantages. They are almost unattended, user-friendly, with relatively economic price, and provide near-real time measurements at high temporal resolution. Furthermore we have also shown (case study in the manuscript) that the intensive optical properties provided by these instruments give information which is more difficult to obtain by means of other instruments at high time resolution (i.e: optical particle counters), such as the identification of mineral dust in the atmosphere after SDE due to regional recirculation. Thus, ground base in-situ optical measurements are really useful to characterize the mineral dust aerosol at surface level and establish relations with air quality.

Despite this, we agree with the Reviewer that, depending on the background atmospheric conditions, not all SDE can be clearly detected using SSAAE or SAE. Presenting these limitations is also one of the aims of this work. In fact, so far, the SSAAE parameter was used for SDE identification at Jungfraujoch station, located at 3580 m.a.s.l., where the SDE detection efficiency was of 100% (Collaud Cohen et al., 2004). Thus, depending on the local conditions, it can be rather difficult to identify a "best indicator" for SDE detection. The synergy between different available tools/instruments (i.e: forecast models, back trajectories analysis, and columnar measurements) is probably the best strategy for a better detection and characterization of these events.

In order to take into account the Referee's comment, the following sentence was added in the Conclusion section:

"Thus, depending on the background atmospheric conditions, not all SDE can be clearly detected using SAE, AAE and SSAAE parameters. And then additional information provided i.e. by forecast models, back trajectories analysis, and columnar measurements is also required in order to better detect and

characterize these events. Nevertheless, aethalometer and nephelometer instruments provide near real time measurements and allow a fast detection of the impact of SDE at ground level. Furthermore, due to the sensitiveness for detecting changes in aerosol size and composition, SSAAE and Angstrom matrix tools are more sensitive compared to other near real-time measurements."

Reviewer#3. General comment 2). This is the same for BB events. What are the end the uncertainities and what do you propose to improve this? Is the present instrumentation enough or is it mandatory to have additional instruments such like ACSM?

Reply to Reviewer#3. General comment 2).

The aethalometer model technique is based on studying the wavelength dependence of aerosol absorption coefficient in order to characterize biomass burning emissions, being this compound a strong absorber in the UV. This technique provides satisfactory estimations of the temporal variability of the contributions for both emission sources, biomass burning and fossil fuel. However, the model presents some limitations for obtaining absolute concentrations. It should be kept in mind that filter sampling artefacts and hypothesis made for assessing OC-to-OM ratios are sources of uncertainty for the Aethalometer model, and these uncertainties are mostly related to the choice of the Ångström exponent.

A larger uncertainty was found for the apportionment of biomass burning to OM (OM_{bb}) compared to BC (BC_{bb}), since there are some organic compounds also absorbing in the UV, such as some aromatic compounds which originates from anthropogenic activities. This fact may lead to a slight overestimation of OM_{bb} due to the overlapping in the UV absorption. Another issue presented in this model is related to the apportionment of biogenic compounds from non-combustion sources, specially in those places with large biogenic emissions and SOA formation, as occurs in our emplacement.

Consequently, it is recommended to carry out simultaneous measurements/experiments applying different techniques not based on optical methods in order to assess the quantification of biomass burning by the model. Some of these techniques have been applied in other studies, such as using levoglucosan as biomass burning tracer, or calibrating the model with the BBOA obtained from applying a source apportionment to ACSM/AMS data, as we did in our study. However, the calibration of the AAE coefficient does not resolve the challenge of discriminating the different compounds absorbing in the UV by optical methods, leading to an overestimation of OM_{bb}.

The differentiation of brown carbon originated from different emission sources by using optical measurements is a challenge, and therefore further analysis using additional techniques for determining biomass burning would be convenient to assess the Aethalometer model performances.

Nevertheless, the aethalometer is a very useful instrument which provides an advantageous technique for real-time air quality monitoring. And then further research in characterizing brown carbon by means of optical techniques is needed in order to exploit the possibilities of the instrument.

In order to consider the reviewer comment, the next sentence was added in the conclusion section of the revised manuscript:

"The differentiation of brown carbon originated from different emission sources by using optical measurements is a challenge, in particular the SOA formation and transformation processes. Due to the uncertainties presented by the aethalometer model for providing absolute concentrations, it is recommended to carry out simultaneous measurements/experiments applying different techniques not based on optical methods, such as using levoglucosan as BB tracer or calibrating the model with BBOA obtained from ACSM source apportionment, in order to assess the quantification of biomass burning by the model. Nevertheless, the aethalometer model is a very useful tool which provides satisfactory estimations of the temporal variability of the contributions for both, biomass burning and fossil fuel emission sources. And then further research in characterizing brown carbon by means of optical techniques is needed in order to exploit the possibilities of the instrument."

Reviewer#3. General comment 3). I also regret that you never present the global amount of aerosol to have an idea of the relative importance of dust or BB aerosol.

Reply to Reviewer#3. General comment 3).

We agree with Reviewer#3, PM concentrations will help to the reader for a better understanding of the article. This issue has been addressed in the specific comment 15.

Figure S1 has been added to the revised supporting material.

Reviewer#3. Specific comment 1). Abstract. Line 18. Here and elsewhere, you never clearly define the "Angstrom matrix".

Reply to Reviewer#3. Specific comment 1).

We agree with the Referee, this definition is missing in the manuscript. The next two sentences will be added to the revised manuscript:

In the abstract: "The Angström matrix (made up by SAE and AAE)"

The sentence was rephrased as follows in section 5.2: "The angstrom matrix is a useful tool to detect periods dominated by SDE (Russell et al. 2010), it consists a scatter plot made up by SAE parameter in the x-axis and AAE parameter in the y-axis, providing information about aerosol size and composition, respectively."

Reviewer#3. Specific comment 2). Line 29: at this stage FF has not been defined.

Reply to Reviewer#3. Specific comment 2).

We agree with the Referee. The next definition has been added to the revised manuscript in the abstract section. "fossil fuel (FF)"

Reviewer#3. Specific comment 3). This high number of acronym sometimes turn to madness, maybe it is useful to have somewhere the list of acronyms.

Reply to Reviewer#3. Specific comment 3).

Excellent suggestion, a list of acronyms containing the most relevant definitions has been added to the supplement information document. The next sentence was added to the manuscript in the introduction section:
"A list of acronyms used in this work is provided in table S1."

Table S1: List of acronyms

Acronym	Definition
AA	Atlantic advections
AAE_{bb}	Fossil fuel absorption Ångström exponent
AAE_{ff}	Biomass burning absorption Ångström exponent

BB	Biomass burning
BBOA	Biomass burning organic aerosol
BC	Equivalent black carbon
BC_{ff}	Equivalent black carbon from fossil fuel source
BC_{bb}	Equivalent black carbon from biomass burning source
FF	Fossil fuel
g	Asymmetry parameter
HOA	Hydrocarbon-like organic aerosol
MSA	Montsec
MSY	Montseny
OM	Organic matter
OM_{bb}	Organic matter from biomass burning source
OM_{ff}	Organic matter from fossil fuel source
PBL	Planetary boundary layer
REG	Regional atmospheric episodes
SAE	Scattering Ångström exponent
SDE	Saharan dust event
SOA	Secondary organic aerosol
SSA	Single scattering albedo
SSAAE	Single scattering albedo Ångström exponent
WMB	Western Mediterranean Basin

Reviewer#3. Specific comment 4). Introduction. Line 25 to 30: I do not understand the logical link "as a consequence" between the two sentences and also I do understand the meaning of the following sentence "Given the huge . . .". I think that this part of the introduction has to be rephrased.

Reply to Reviewer#3. Specific comment 4).

The expression "as a consequence" was suppressed and the text has been edited as follows: "These intensive properties present a valuable input for climate models, which require accurate information concerning the variability of atmospheric composition for targeted species via comparison with observations (Laj et al., 2009)."

Reviewer#3. Specific comment 5). Line 12: Is Spain often having exceedances compared to other European countries?.

Reply to Reviewer#3. Specific comment 5)

In this paragraph we are highlighting the importance of SDE effects on air quality, and therefore the necessity of detecting SDE in near-real time. As is detailed in the text, southern European countries are frequently affected by SDE. In fact, in Spain dust outbreaks lead to the 70% of the exceedances in the PM_{10} daily limit value (Escudero et al., 2007a) at most regional background sites in Spain. Then, Spain often present exceedances in the PM_{10} daily limit value due to Saharan dust outbreaks, compared to other northern European countries which are distant from African dust sources, and then SDE does not present important effects on air quality.

Reviewer#3. Specific comment 6). Chapter 3, P7 line 14 "assess".

Reply to Reviewer#3. Specific comment 6)

It has been corrected.

Reviewer#3. Specific comment 7). P7, line 19: Maybe you need to tell more about the results of Russell et al (2010).

Reply to Reviewer#3. Specific comment 7)

What we found missing in this sentence, referring to the work presented by Russell et al. (2010), is to mention that data analyzed in that work was obtained from columnar measurements, whereas our work was performed at ground level. Accordingly to the Referee's suggestion, the sentence in section 3 has been modified as follows:

"Russell et al. (2010) has also performed the AAE and SSAAE parameters for full aerosol vertical columns obtained from sun-sky photometer retrievals, in order to characterize aerosol columns dominated by the two important sources of UV absorbing aerosols, biomass burning and Saharan dust."

Reviewer#3. Specific comment 8). Finally, and it is link to one of the general remark, you would say that the methodology for SDE only works for altitude (very remote sites)?.

Reply to Reviewer#3. Specific comment 8).

Answer to this question is further developed in the general comment #1.

In this work we have shown that the intensive optical properties present some limitations for characterizing atmospheric aerosols, however these properties may be calibrated for each sampling site for a better performance of the results. The detection of SDE mainly depends on the emplacement background pollution and the intensity of the event, and then a larger mixture of mineral dust with anthropogenic pollutants will prevent a change in the spectral dependence of scattering and absorption. The smaller size of anthropogenic pollutants unified to the black colour provided by the combustion emission sources, turns into positive values the spectral dependence of the SSA.

Therefore a better detection of SDE by means of using the intensive optical properties will be performed in those sites less influenced by anthropogenic emission sources. However, the best approach is to combine all available tools in order to: first, predict the SDE by performing mineral dust and meteorological forecast models; second, detect the mineral dust layer before the plume reaches to the ground by performing remote data from lidar/ceilometer, sun-photometer and/or satellite products; and finally, characterize the impact of mineral dust at ground level by the performance of ground measurements.

Reviewer#3. Specific comment 9). P8 line 7 "in this work" which one? Minguillón et al? then do no go to the line.

Reply to Reviewer#3. Specific comment 9).

"In this work" refers to the study that is being presented in this manuscript. In order to avoid confusions, the expression has been replaced by the next one: "In the present work".

Reviewer#3. Specific comment 10). Chapter 5, P9, line 2 to 8. There is something confusing in these lines, you compare SAE at MSA (altitude) and MSY (near Barcelona) and you say that SAE is greater at MSA because it is often within the BDL but probably not as often as MSY I guess. In line 4 you have to give some elements about the fact that we have smaller and darker particles at mountain sites. Line 6-7-8 I do not understand your analysis, I do not know what is compared to what.

Reply to Reviewer#3. Specific comment 10).

Line 2 to 8: Previous studies have shown that under low aerosol loadings at mountain top sites the aerosol mixture is preferentially composed of relatively smaller and darker particles (i.e Pandolfi et al., Andrews et al., and references therein). A larger SAE at MSA is probably due to the frequent position of the station within the free troposphere (FT) (above the PBL (planetary boundary layer)), predominantly in winter. However, MSY which is located at lower altitude and more frequently within the PBL, shows slightly lower SAE probably due to the influence of a more polluted background environment.
It may be possible that Referee#3 has misunderstood the sentence in the manuscript: "Mean SAE was higher at MSA station compared to MSY, which could be explained by a dominance of smaller particles on average at MSA likely due to frequent position of the station within the free troposphere in winter."

Line 4: Previous studies at MSA site have described the free troposphere conditions, occurring almost during the colder period and characterized by a marked reduced PM concentrations (Ripoll et al., 2014). A more detailed analysis relating FT conditions and optical properties at MSA was performed by Pandolfi et al. (2014a). This study showed that under very low PM_1 concentrations (<1.5 µg m^{-3}) at MSA, SSA and g parameters reached very low values around 0.84 and 0.43 respectively, whereas the SAE increased (Figure 6 in Pandolfi et al. 2014a). These low PM conditions at MSA were related to the prevalence of small particles with relatively higher absorption properties regardless of the considered atmospheric scenario. Low values of SSA at very low aerosol loading have been observed at other mountain top sites (i.e. Andrews et al. (2011) and references therein), and were related with an aerosol mixture in which large aerosol scattering particles have been preferentially removed (e.g. by cloud scavenging and/or deposition), leaving behind a relatively smaller and darker aerosol.

In order to take into account the referee's comment, the paragraph was rephrased as follows in section 5.1 of the revised manuscript:

"As already reported (Andrews et al., 2011; Berkowitz et al., 2011; Marcq et al., 2010; Pandolfi et al., 2014a), under low aerosol loadings at mountain top sites, in which large aerosols scattering particles have been preferentially removed, the aerosol mixture is mainly composed of relatively smaller and darker particles. Previous studies at MSA have described the free troposphere conditions, characterized by very low PM_1 concentrations (<1.5 µg m^{-3}), low values of SSA (0.83) and g (0.43) parameter, and increasing SAE (Pandolfi et al., 2014a)."

Line 6-7-8: In order to avoid confusion, the sentence was rephrased as follows:
"MSY site presented slightly lower AAE values compared to MSA, due to a major predominance of black carbon particles as a consequence of the proximity to Barcelona urban area."

Reviewer#3. Specific comment 11). P9 line 9: do you have an analysis to propose about relative SSA values at each sites?

Reply to Reviewer#3. Specific comment 11).

Previous works focused on studying optical properties at MSY and MSA were performed by Pandolfi et al. (2011 and 2014a, respectively), and SSA values were analysed in these studies. For this reason, and also due to the fact that the intensive optical properties presented in our work aimed to detect specific atmospheric scenarios (SDE and BB events), we have not considered further analysis on SSA.

Reviewer#3. Specific comment 12). P9 line 17: maybe define the "angstrom matrix" term.

Reply to Reviewer#3. Specific comment 12).

We agree with the Referee. The text has been edited as follows:

"The angstrom matrix is a useful tool to detect periods dominated by SDE (Russell et al., 2010), it consist of a scatterplot made up by SAE parameter in the x axis and AAE parameter in the y axis, providing information about aerosol size and composition, respectively. The scatterplot can be colour coded and investigated by other parameters in order to further characterize the atmospheric aerosols. In our case the matrix was colour coded by different air mass origin and by the coarse fraction contained within the PM_{10} (%PM_{1-10} in PM_{10}), which was calculated as the difference between %PM_1 and %PM_{10} contained within the PM_{10} fraction."

Reviewer#3. Specific comment 13). P9 line 18 : I think you never define what is PM1-10 , even if I can guess it is better to define it .

Reply to Reviewer#3. Specific comment 13).

Following the referee's suggestion, the revised manuscript has been modified as is detailed in the previous answer:

"In our case the matrix was colour coded by different air mass origin and by the coarse fraction contained within in the PM_{10} (%PM_{1-10} in PM_{10}), which was calculated as the difference between %PM_1 and %PM_{10} contained within the PM_{10} fraction."

Reviewer#3. Specific comment 14). P9 line 21: I would have prefer "situation" than "scenario"

Reply to Reviewer#3. Specific comment 14).

It has been changed; "scenario" was replaced by "situation".

Reviewer#3. Specific comment 15). P9 line 22-23: the limits you are mentioning are not that clear, it seems to me that there is an important mixing of the different "scenario" even if some patterns are indeed emerging. It would interesting to have the statistics of the nb of points within the limits of SAE and AAE for SDE and also for other situations. A more quantitative way to evaluate this aspect.

Reply to Reviewer#3. Specific comment 15).

We agree with Referee#3, a quantitative analysis of SAE and AAE parameters for the different atmospheric situations should be added to the manuscript for a better performance of the intensive optical properties. However, it should be considered that data within the Ångström matrix is displayed on hourly

base whereas air mass origin was identified once per day, therefore daily average values may include some hourly data points which are not representing entirely these situations.

In order to consider this comment, the general comment #3 and the specific comment #2 from Referee#2 regarding this issue, figure S1 has been added to the revised supporting material. These figures show the frequency distribution of SAE, AAE, PM_{10} (µg m^{-3}) and %PM_{1-10} in PM_{10} for the different atmospheric scenarios (SDE, REG and AA), at MSY and MSA respectively. These plots will help to the reader to interpret the variability of the intensive properties and establish differences among atmospheric scenarios at both stations. In addition, the following sentences were added to section 5.2 in the revised manuscript:

"Average and standard deviation of SAE and AAE during SDE were 1.12±0.87 and 1.27±0.24 for MSY, and 0.69±0.78 and 1.41±0.25 for MSA. Lower SAE and higher AAE at MSA pointed to a larger dominance of mineral dust and a purer composition during these events at the high altitude station (Fig. S1). Average PM_{10} concentrations during SDE were 25.4±17 and 21.0±17 µg m^{-3} for MSY and MSA respectively. Further information providing the frequency distribution and average values of SAE, AAE, PM_{10} and %PM_{1-10} in PM_{10} for each atmospheric situation at both stations is reported in Fig. S1."

"Average and standard deviation of SAE and AAE during these scenarios were 1.35±0.95 and 1.33±0.27 for MSY, and 1.65±0.57 and 1.30±0.16 for MSA, respectively. PM_{10} showed the lowest concentrations during these events, being 11±7 and 9.4±6 µg m^{-3} respectively for MSY and MSA (Fig. S1)."

"SAE and AAE values during REG episodes were 1.61±0.87 and 1.24±0.19 for MSY, and 1.66±0.48 and 1.29±0.15 for MSA, respectively. The average PM_{10} concentrations during these atmospheric situations were 15.6±8 and 12.6±7 µg m-3.for MSY and MSA (Fig. S1)."
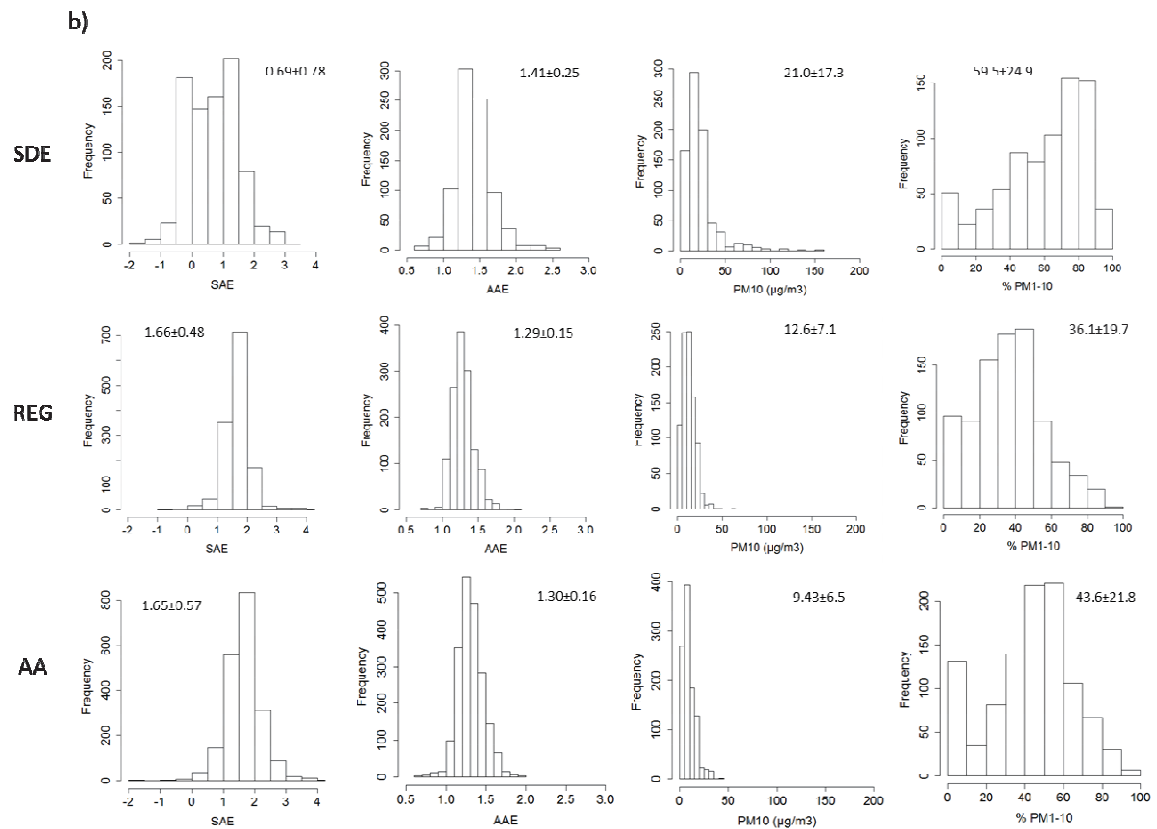
b)
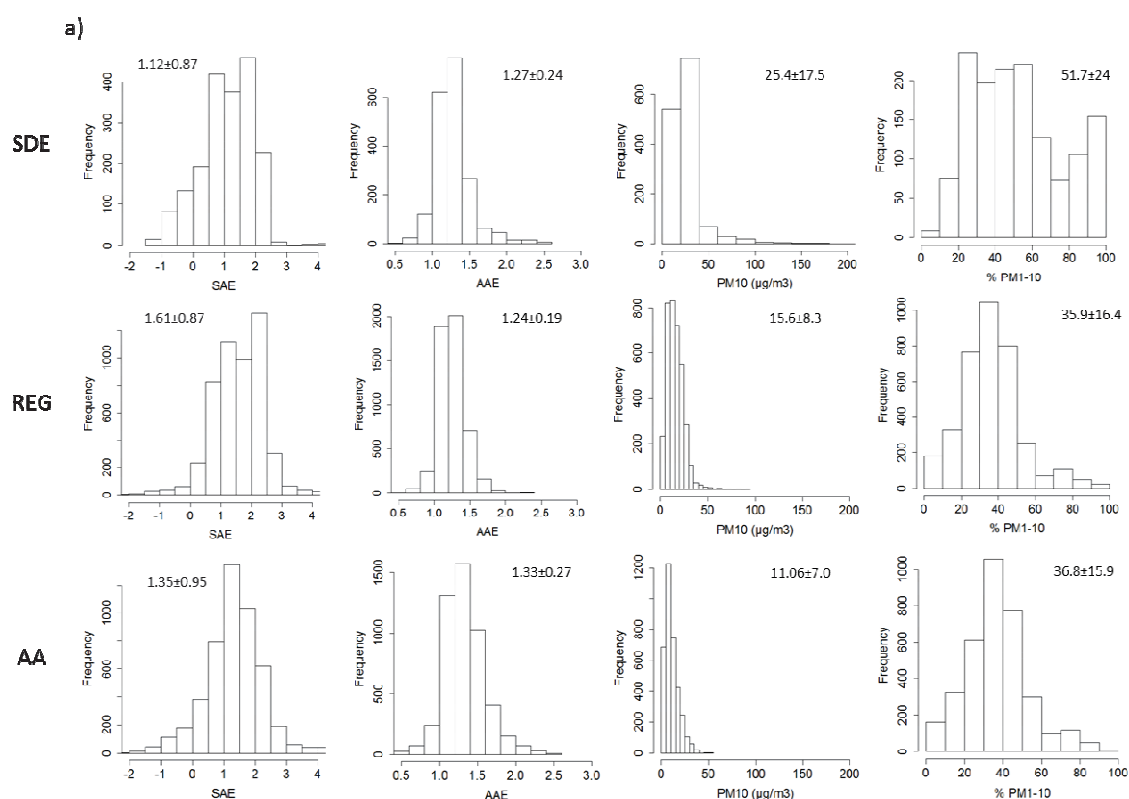
Figure S1. Frequency distribution, average and standard deviation of SAE, AAE, PM_{10} and %PM_{1-10} in PM_{10} parameters for the three atmospheric scenarios (SDE, REG, AA) displayed in the Ångström matrix at (a) MSY and (b) MSA.

Reviewer#3. Specific comment 16). P10 line 5-15 once more you are speaking of the fact that we have finer particles at mountains top for example for AA situations (you definitively have to explain why I think) and on the other hand you are saying that we also have finer particles during REG due to pollution. Is it meaning that we cannot distinguish? just PM concentrations help to decide this probably. You have to clarify the discussion and the objectives of the discussion.

Reply to Reviewer#3. Specific comment 16).

Definitely, Table S1 added to the supporting material is necessary for a better understanding of the intensive optical properties variation within the different atmospheric situations.

As we have discussed in specific comment #10, the high altitude MSA station is frequently located within the free troposphere during the colder period. The low temperature during this period restrict the atmospheric convection processes leading to a less growing of the PBL, and then, as a result the PBL height is lower than the altitude of the station (1570 m a.s.l.), which remains within the free troposphere. Free troposphere conditions at MSA can occur during both, AA and REG atmospheric situations taking place during winter, although AA (65%) scenarios are most common in this time of the year compared to REG (10%) (Ripoll et al., 2014).

Therefore, SAE and AAE parameters are very similar at MSA and only can be differentiated by PM_{10} concentration (Fig. S1). PM_{10} tail distribution is slightly shifted towards larger concentrations during REG compared to AA scenarios. However differences at MSY between both atmospheric situations are more evident, SAE at MSY present larger values during REG compared to AA episodes. It is also reflected in the PM_{10} distribution which presents larger values during REG.

Following these results, we totally agree with the Referee#3 that PM_{10} concentration provide valuable information and should be considered to establish differences among different atmospheric scenarios. Despite SAE values for AA and REG episodes are quite similar; the PM_{10} concentrations mark the difference. REG episodes are related to pollution scenarios and show a higher average PM_{10} concentration (12.6 and 15.6 µg m^{-3} at MSA and MSY), whereas AA clears out the atmosphere leading to lower background concentrations (9.4 and 11.0 µg m^{-3} at MSA and MSY).

Reviewer#3. Specific comment 17). P10 line 7-8 what kind of aerosol concentrations are we speaking of?

Reply to Reviewer#3. Specific comment 17).

Regarding to specific comments #16 and #17, the table S1 has been added to the revised supporting material. Frequency distribution and average values of SAE, AAE, PM_{10} and $\%PM_{1-10}$ in PM_{10} are provided for the three atmospheric scenarios (SDE, REG, AA) displayed in the Ångström matrix. Average PM_{10} concentrations during AA scenarios were 11.0 and 9.4 µg m^{-3} at MSY and MSA sites, respectively.

Reviewer#3. Specific comment 18). P11 line 11-20 : the analysis of this episodes has to be reinforce. More than supposition, you must present facts of this recirculation event using meteorological information. You are speaking often of this case with strong conclusion then you have to give more evidence to readers.

Reply to Reviewer#3. Specific comment 18).

In order to better characterize the regional recirculation scenario, the dust forecast image from Dream model was added to Fig. S3 in the revised supporting material (Fig. S3d).

The SDE is clearly identified by the air mass origin from North Africa (Fig S3a) and is further confirmed by the Dream model pointing to 20-40 µg m^{-3} of dust surface concentration (Fig. S3c). The air mass origin during REG episode on 1/11/2013, occurring after the SDE, shows the stagnation of air masses with a very local and regional origin (Fig S3b). However, despite the intensive optical parameters show the presence of mineral dust during the REG episode with SSAAE<0 and the corresponding decreasing SAE and increasing AAE (Fig. 3d in the manuscript), the Dream model is not able to predict the resuspension of mineral dust (Fig. S3d).
PM_{10} data is not available for this case study in order to evaluate PM_{10} concentrations during the SDE and REG episode. We cannot further characterize the REG episode with the available observational data.
It would be interesting to carry out a simulation at high spatial resolution in order to better characterize the regional air masses leading the re-circulation of mineral dust. In fact, it would be interesting to deploy a study focused on the characterization of these re-circulation scenarios in order to better evaluate the effects on air quality, but we did not consider implementing high computing time simulations in this study.
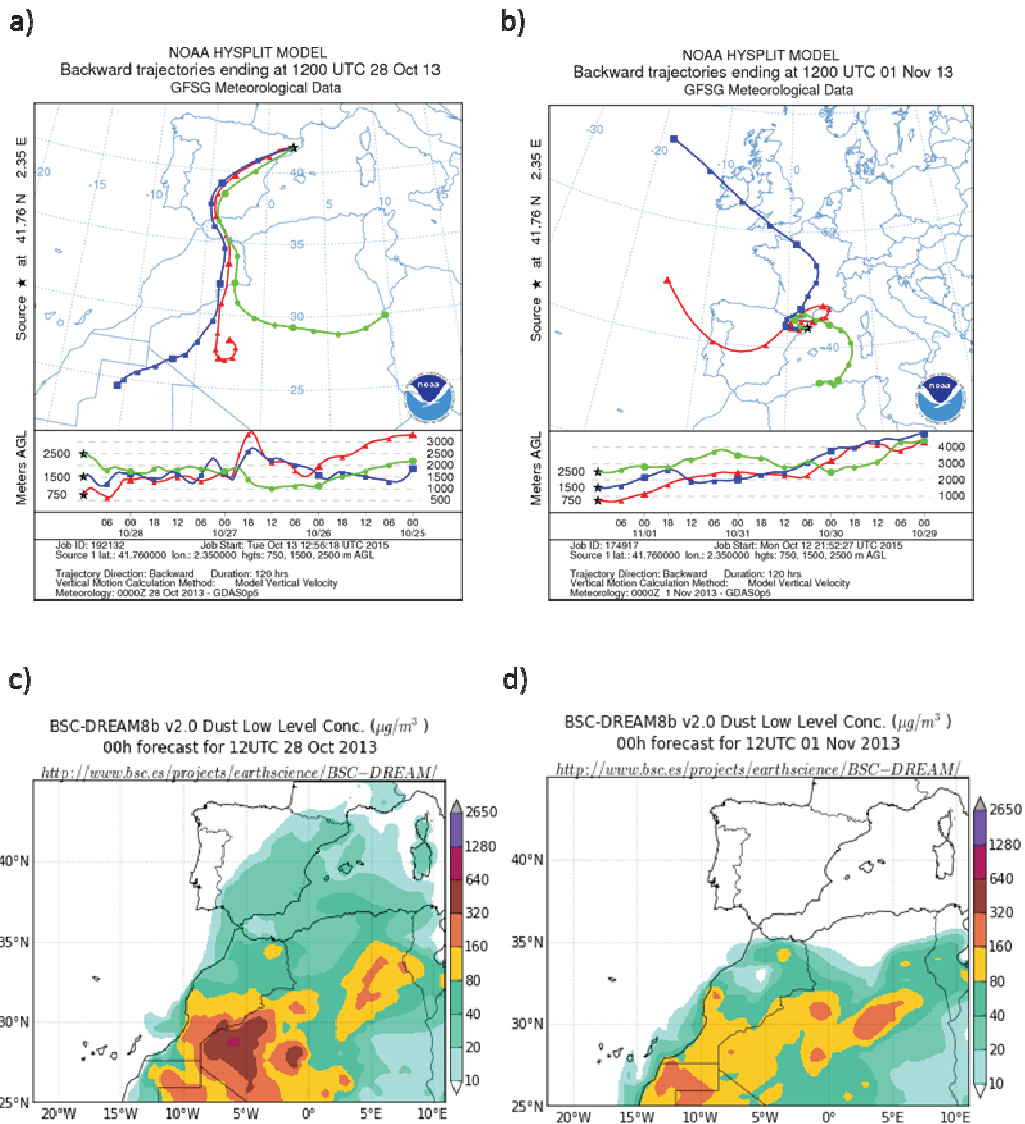
Figure S3. Backward trajectories corresponding to (a) the Saharan dust event (28/10/2013) and (b) the regional episode (01/11/2013) atmospheric scenarios at MSY. Dust surface concentration at MSY from the Dream model corresponding to (c) the Saharan dust event (28/10/2013) and (d) the regional episode (01/11/2013).

Accordingly to referee's suggestion the next text was added to section 5.2 of the manuscript:

"It is interesting to highlight that despite the intensive optical parameters showed the presence of mineral dust during the REG episode, with SSAAE<0 and the corresponding decreasing SAE and increasing AAE, the Dream was not able to reproduce the recirculation of mineral dust (Fig. S3d), and only a simulation at high spatial resolution could characterize the event."

Reviewer#3. Specific comment 19). P13 line 12 : also less VOC emissions during winter no ?

Reply to Reviewer#3. Specific comment 19).

We agree with the Referee, the lower SOA formation in winter is mainly leaded by a less concentration of VOCs, which are one of the primary precursor sources of SOA formation during the warmer period in this emplacement (Seco et al. 2013).

The sentence will be rephrased as follows in the revised manuscript:

"The slope was close to the unity due: to the lower SOA formation in winter, mainly explained by a decreasing of VOCs emissions being one of the primarily precursor sources of SOA formation during the warmer period in this emplacement (Seco et al., 2013), and also as consequence of less photochemistry activity and the prevalence of primary emissions."

Reviewer#3. Specific comment 20). P13 line 4-7 : is there not a contradiction within this sentence ? I have the impression you are saying one thing (low values of AAE during the day) and its contrary (increase of AAE during warmest hours of the day) . . .

Reply to Reviewer#3. Specific comment 20).

We agree with the referee, there is a mistake in this sentence which leads to a contradiction regarding the daily cycle of AAE. The sentence was rephrased as follows:

"Low values of AAE during the day and higher at night at both sites resulted mainly from the development of sea and mountain breezes, favouring the transport of anthropogenic pollutants from the urbanized/industrialized coastline and valleys to inland areas and leading to a decrease of AAE during the warmest hours of the day (Fig. 6a).

Reviewer#3. Specific comment 21). P14 line 16 : "noted"

Reply to Reviewer#3. Specific comment 21). It has been corrected

Reviewer#3. Specific comment 22). P15 line 3-5: you suppose having less BB during night because of a thermal inversion above residual layer but is BB not also associated to domestic heating during colder hours i.e during the night which would imply that this BB would be trapped within the thin night BDL.

Reply to Reviewer#3. Specific comment 22).

We did not suppose having less BB during night. What we suppose in these lines is that OM_{bb}, which started increasing during the afternoon, remained stable during night and did not showed much variation (but the concentration was still high during night). This fact may be explained by the decrease of the PBL and the formation of the typical thermal inversion at lower levels during night, which may imply that the biomass burning emitted during the previous hours was trapped above the thermal inversion in the residual layer.
We agree with the Referee that BB concentration should increase within the night boundary layer as a result of domestic heating activities. However, since the station is located at higher altitude than emission sources (houses), we suppose that the BB we are measuring at night is trapped within the residual layer.

Detection of Saharan dust and biomass burning events using near real-time intensive aerosol optical properties in the northwestern Mediterranean.

Marina Ealo[1][2], Andrés Alastuey[1], Anna Ripoll[1], Noemí Pérez[1], Maria Cruz Minguillón[1], Xavier Querol[1] and Marco Pandolfi[1].

[1] Institute of Environmental Assessment and Water Research (IDAEA-CSIC), Barcelona, Spain
[2] Department of Astronomy and Meteorology, Faculty of Physics, University of Barcelona, Spain

Correspondence *to*: Marina Ealo (marina.ealo@idaea.csic.es)

Abstract. The study of Saharan dust events (SDE) and biomass burning (BB) emissions are both topic of great scientific interest since they are frequent and important polluting scenarios affecting air quality and climate. The main aim of this work is evaluating the feasibility of using near real-time in situ aerosol optical measurements for the detection of these atmospheric events in the Western Mediterranean Basin (WMB). With this aim, intensive aerosol optical properties (SAE: scattering Ångström exponent, AAE: absorption Ångström exponent, SSAAE: single scattering albedo Ångström exponent, and g: asymmetry parameter) were derived from multi-wavelength aerosol light scattering, hemispheric backscattering and absorption measurements performed at regional (Montseny; MSY, 720 m a.s.l.) and continental (Montsec; MSA, 1570 m a.s.l.) background sites in the WMB. A sensitivity study aiming at calibrating the measured intensive optical properties for SDE and BB detection is presented and discussed.

The detection of Saharan dust events (SDE) by means of the SSAAE parameter and Ångström matrix (made up by SAE and AAE) depended on the altitude of the measurement station, and on SDE intensity. At MSA (mountain-top site) SSAAE detected around 85% of SDE compared with 50% at MSY station, where pollution episodes dominated by fine anthropogenic particles frequently masked the effect of mineral dust on optical properties during less intense SDE. Furthermore, an interesting feature of SSAAE was its capability to detect the presence of mineral dust after the end of SDE. Thus, resuspension processes driven by summer regional atmospheric circulations and dry conditions after SDE favored the accumulation of mineral dust at regional level having important consequences for air quality. On average, SAE, AAE and *g* ranged between -0.7 and 1, 1.3 and 2.5, and 0.5 and 0.75, respectively, during SDE.

Based on the Aethalometer model, biomass burning (BB) contribution to equivalent black carbon (BC) accounted for 36% and 40% at MSY and MSA respectively. Linear relationships were found between AAE and $\%BC_{bb}$, with AAE values reaching around 1.5 when $\%BC_{bb}$ was higher than 50%. BB contribution to organic matter (OM) at MSY was around 30%. Thus fossil fuel (FF) combustion sources showed important contributions to both BC and OM in the region under study. Results for OM source apportionment showed good agreement with simultaneous biomass burning organic aerosol (BBOA) and hydrocarbon-like organic aerosol (HOA) calculated from Positive Matrix Factorization (PMF) applied to simultaneous Aerosol Mass Spectrometer (ACSM) measurements. A wildfire episode was identified at MSY, showing AAE values up to 2 when daily BB contributions to BC and OM were 73% and 78% respectively.

1. Introduction

Atmospheric aerosols play an important role in our environment affecting air quality and health (Pope and Dockery, 2006), contributing to the largest uncertainties to the total radiative forcing (IPCC 2007, 2013). Aerosol affects climate by perturbation on the Earth's radiative budget, directly through absorption and scattering of solar and terrestrial radiation, and indirectly by acting as cloud condensation nuclei (Twomey et al., 1984; Albrecht, 1989). Most particles scatter the sunlight, causing a net cooling at the top of the atmosphere (TOA), whereas black carbon (BC) absorbs solar radiation in the whole

visible spectrum, thus causing a net warming at the TOA (Jacobson, 2001; Ramanathan and Carmichael, 2008; Bond et al., 2013). Absorbing particles can modify the radiation fluxes directly, by absorption of shortwave solar radiation and semi-directly, by modifying the temperature distribution of the atmosphere. Absorption in the UV range is important, since it may affect photo-chemistry thus reducing tropospheric ozone concentration (Jacobson, 1998; Chen and Bond, 2010). Mineral matter and some organic compounds mainly from biomass burning (BB) emissions, called brown carbon (BrC), can also absorb solar radiation in the UV range of the solar spectrum. BrC contains a large and variable group of organic compounds including humic substances, polyaromatic hydrocarbons, and lignin (Andreae and Gelencsér, 2006), and it is formed by inefficient combustion of hydrocarbons (biomass burning) and also by photo-oxidation of biogenic particles (Yang et al., 2009). The light absorption by mineral dust depends on its content of ferric oxides (Sokolik and Toon, 1999; Alfaro et al., 2004).

Thus, the study of the relationship between physicochemical and optical properties of aerosols is strongly required in order to obtain a deeper characterization of atmospheric aerosols and therefore a better estimation of their radiative forcing. Some parameters can be derived from multi-wavelength scattering and absorption aerosol measurements in order to describe the optical properties as a function of the wavelength. These parameters, such as single scattering albedo (SSA), asymmetry parameter (g), scattering Ångström exponent (SAE), absorption Ångström exponent (AAE) and single scattering albedo Ångström exponent (SSAAE), are determined by the physicochemical properties of aerosols and are called intensive because do not depend on the particle mass. These intensive As a consequence the intensive aerosol optical properties are present a valuable input for climate models, which require accurate information concerning the variability of atmospheric composition for targeted species via comparison with observations (Laj et al., 2009). Given the huge variety of aerosol emission sources and formation and transformation processes, there is a substantial need of accurate real-time aerosol optical measurements to achieve a low-error estimation of the effects that atmospheric particles have on climate coupling experimental measurements and modelling results (IPCC, 2007; 2013).

In order to get a wide coverage of the spatial variability of aerosols, aerosol optical data are obtained all over the world from both in situ and remote measurements. The in situ optical measurements are usually performed in international networks by means of automatic instruments which provide real-time data at high temporal and spatial resolution. Some of the most relevant networks are Aerosols, Clouds and Trace Gases Research InfraStructure (ACTRIS; www.actris.net), Global Atmospheric Watch (GAW; www.gaw-wdca.org), Aerosol Robotic Network (AERONET; www.aeronet.gsfc.nasa.gov) and NOAA baseline observatory (www.esrl.noaa.gov).

The WMB is affected by a large variety of emissions sources: natural sources such as Saharan dust, marine aerosols and wildfire; industrial and urban emissions from densely populated areas in the coastline; and transboundary from the European continent (Steinbrecher et al., 2009; Rodríguez et al., 2011; Pey et al., 2013a , 2013b; Garcia-Hurtado et al., 2014). The atmospheric dynamics coupled to local orography gives rise to a complex mixture of pollutants (Millán et al., 1997) where aerosol formation and transformation processes take place and accumulation of pollutant is very frequent (Rodríguez et al., 2002, 2003; Pérez et al., 2004; Jiménez et al., 2006; Pey et al., 2010; Jorba et al., 2013; Pandolfi et al., 2014b). Furthermore, the high occurrence of Saharan dust events (SDE), especially during the summer period, also contribute strongly to the increment of PM_{10} levels in the WMB (Rodríguez et al., 2001, 2015; Querol et al., 2009; Pey et al., 2013a). In fact, more than 70 % of the exceedances of the PM10 daily limit value (2008/50/CE European Directive) at most regional background sites of Spain have been attributed to dust outbreaks (Escudero et al., 2007a). Thus, all these processes lead to a radiative forcing in the WMB among the highest in the word (Jacobson, 2001). Nevertheless there is a large uncertainty in the total radiative forcing by atmospheric aerosols in the Mediterranean area (Mallet et al., 2013). The high occurrence and intensity of SDE in the WMB give us the opportunity to look deeply into the characterization of the optical properties of mineral dust when mixed with local aerosols. Despite several studies published on physical and chemical properties of mineral dust in the

WMB region (Rodríguez et al., 2001; Escudero et al., 2007b; Querol et al., 2009; Pey et al., 2013a), very few have studied how SDE affect the aerosol intensive optical properties (Pandolfi et al., 2011 and 2014a; Valenzuela et al., 2015)

Possibly related to the scarce use of biomass burning for domestic heating in the Mediterranean region compared to Central and Northern Europe, very few studies have been published describing BrC effects on intensive aerosol optical properties in the WMB. However, recent studies have estimated that biomass burning sources in the WMB may contribute more than expected to the measured ambient elemental carbon (EC) and organic carbon (OC) concentrations (Minguillón et al., 2011 and 2015; Reche et al., 2012; Mohr et al., 2012; Viana et al., 2013; Pandolfi et al., 2014b). In these studies the biomass burning source was characterized by means of techniques such as positive matrix factorization (PMF) on AMS (Aerosol Mass Spectrometer) or ACSM (Aerosol Chemical Speciation Monitor) data, filter-based analysis of 14C and/or specific chemical tracers such as levoglucosan or K+. Nevertheless, only few studies have used multi-wavelength Aethalometer data (Sandradewi et al., 2008b) in the WMB (Segura et al., 2014).

The main aim of this work is to provide a deep characterization of the intensive optical properties of atmospheric aerosols in the WMB under specific pollution episodes (SDE and BB). Thus, here we evaluate the feasibility of using the intensive aerosol optical properties for the near real-time detection of specific atmospheric events in the WMB. A sensitivity study aimed at calibrating the measured intensive aerosol optical properties is presented and discussed. We show that this calibration is needed to take into account the effects of local pollution on the intensive optical properties during SDE and BB events. Moreover, we provide the range of variability of the calculated intensive optical properties as a function of the intensity of these events. This information is a valuable input for models studying the radiative effects of atmospheric aerosols in this very peculiar area. With this aim we used high-quality data collected at two stations located in the WMB: Montseny (MSY, regional background station; 720 m a.s.l.) and Montsec (MSA, remote station; 1500 m a.s.l.). A list of acronyms used in this work is provided in table S1.

2. Methodology

2.1 Sampling sites

Results presented in this study were obtained from data collected at two in situ measurement stations located in the NE Iberian Peninsula (Fig. 1). The Montseny (MSY) site, integrated in the ACTRIS (Aerosol, Clouds and Trace gases Research InfraStructure) network, is a middle altitude emplacement (720 m a.s.l.) representative of the regional background in the WMB. The MSY measurement station is located in the Montseny Natural Park (41°19'N, 02°21'E), 40 Km to the NNE of the Barcelona urban area and 25 km from the Mediterranean coast, and is frequently affected by anthropogenic emissions (Pérez et al., 2008). The continental background site Montsec (MSA), integrated in the GAW (Global Atmosphere Watch) programme, is a remote high altitude emplacement (1570 m a.s.l.) situated in the southern side of the Pre-Pyreness at the Montsec d'Ares mountain (42°3'N, 0°44'E), 140 km to the NW of Barcelona and 140 Km to the WNW of Montseny (Ripoll et al., 2014). In situ optical aerosol properties measured at these two sites were performed following the standards required by GAW and ACTRIS networks.

Detailed information on these monitoring stations can be found for example in Pérez et al. (2008), Pey et al. (2009), Pandolfi et al. (2011), Cusack et al. (2012), and Minguillón et al. (2015) for MSY, and in Ripoll et al. (2014, and 2015b), Pandolfi et al. (2014a) for the MSA site.

2.2 Classification of atmospheric scenarios

The classification of atmospheric episodes affecting MSA and MSY sites on each day of the sampling period was performed following the procedure described by Ripoll et al. (2014) using BSC-DREAM8b (Basart et al., 2012), SKIRON (Nickovic et al., 2001) and HYSPLIT (Draxler and Rolph, 2015; Rolph 2015) models.

A detailed description of the main meteorological processes affecting the area under study can be found in Pérez et al., (2008); Pey et al., (2010); Pandolfi et al., (2014a); Ripoll et al., (2014). This study is focused in the atmospheric scenarios affecting significantly the concentrations of pollutants in the WMB: North African (NAF), summer regional (REG) and Atlantic advections (AA). SDE, driven by NAF air masses, are more frequent from March to October strongly contributing to increase PM_{10}. The summer REG scenarios favour the dispersion of the pollutants around the emission sources and the transport and accumulation of pollutants through the regional recirculation of air masses (Millán et al., 1997). Often REG occur after SDE causing important effects on air quality as shown later. Atlantic advections (AA) affect the WMB throughout the year but mainly in winter. Fresh and clean air masses from the Atlantic clear out the previously accumulated stagnated air masses, leading to lower pollutant concentrations at regional scale. The seasonal distribution of the main atmospheric episodes throughout the year is very similar at MSY and MSA. However, during colder periods MSA high altitude station is frequently within the free troposphere conditions whereas MSY station is frequently affected by regional/local emission sources being often within the planetary boundary layer PBL (Pandolfi et al., 2014 a, b).

The African dust contribution to PM_{10} (%dust) at MSY was calculated by the statistical methodology described in Escudero et al. (2007b) and Pey et al. (2013). This method is based on the application of 30 days moving 40th percentile to the daily PM_{10} data series, after excluding those days impacted by African dust. For those days affected by African dust the percentile value is assumed to be the theoretical background concentration of PM if African dust did not occur. After that, the African dust daily contribution is obtained as the difference between the experimental PM_{10} concentration and the calculated 40th percentile value.

2.3 Measurements and instrumentation

2.3.1 Aerosol absorption and Equivalent black carbon (BC) concentration measurements

Aerosol light absorption coefficient (σ_{ap}) at 637 nm (Müller et al., 2011a) was measured at 1 min resolution with a Multi Angle Absorption Photometer (MAAP, model 5012, Thermo). BC mass concentrations (Petzold et al., 2013) were calculated assuming a constant mass absorption cross section (MAC) of 6.6 m^2 g^{-1} (Petzold and Schönlinner, 2004). The detection limit of the MAAP instrument is lower than 100 ng m^{-3} over 2 min integration.

Aerosol light absorption coefficients (σ_{ap}) at seven different wavelengths (370, 470, 520, 590, 660, 880 and 950 nm) were obtained every 1 min at both stations by means of Aethalometer instruments (models AE-31 and AE-33). At MSA site the AE-33 (Drinovec et al., 2015) was equipped with a $PM_{2.5}$ cut-off inlet until March 2014 and with a PM_{10} cut-off inlet afterwards. Absorption measurements at MSY station were carried out with a PM_{10} cut-off inlet using an AE-31 Aethalometer model from June 2012 to June 2013, then replaced with an AE-33 model. Absorption measurements from the AE-31 were corrected for loading and scattering effects according to Weingartner et al. (2003). The site-specific AE-31 multiple scattering correction factor (C) at MSY was obtained by comparing with measurements from MAAP and it was estimated in around 3.6. Data was normalized to standard conditions (273K, 1013 hPa). Multi-wavelength aerosol absorption measurements used in this work cover a period of 2.5 year at MSY (June 2012-December 2014) and around 1 year at MSA (November 2013-December 2014).

2.3.2 Aerosol scattering measurements

Aerosols light scattering (σ_{sp}) and hemispheric backscattering (σ_{bsp}) coefficients were measured at each site every 5 min at three different wavelengths (450, 525 and 635 nm) with a LED-based integrating nephelometer (model Aurora 3000, ECOTECH Pty,Ltd, Knoxfield, Australia). Calibration of the nephelometer was performed three times per year by using CO_2 as span gas while zero adjusts were performed once per day by using internally filtered particle free air. A relative humidity (RH) threshold was set following the ACTRIS recommendations (RH<40%). Scattering measurements were corrected for truncation due to non-ideal detection of scattered radiation following the procedure described in (Müller et al., 2011b).

Multi-wavelength aerosol scattering measurements used in this work cover a period of 5 years at MSY (from January 2010 to December 2014) and 3.5 years at MSA (from July 2011 to December 2014).

2.3.3 PM measurements

Real-time PM concentrations were continuously measured at 30 and 5 min resolution by optical particle counters (OPC) using GRIMM spectrometers (GRIMM 180 at MSY, and GRIMM 1107 and GRIMM 1129 at MSA). Concentrations were corrected by comparison with 24 h gravimetric mass measurements of PMx (Alastuey et al., 2011). For gravimetric measurements 24h PMx samples were collected every 4 days on 150 mm quartz micro-fiber filters (Pallflex QAT) with high-volume (Hi-Vol) samplers (DIGITEL DH80 and/or MCV CAV-A/MSb at 30 m^3 h^{-1}).

3. Calculation of the intensive aerosol optical properties

The extensive and intensive aerosol optical properties and the equations used to derive the intensive properties are reported in Table 1 and briefly commented below.

In order to study some of the aforementioned intensive optical properties over a wider spectral range, the 3λ scattering measurements from nephelometer were derived at the 7 Aethalometer wavelengths using the SAE calculated from 3λ measured scattering. Once scattering was obtained at the 7λ, we estimated SSA and SSAAE at these 7λ.

The extensive and intensive aerosol optical properties and the equations used to derive the intensive properties are reported in Table 1 and briefly commented below.

In order to study some of the aforementioned intensive optical properties over a wider spectral range, the 3λ scattering measurements from nephelometer were derived at the 7 Aethalometer wavelengths using the SAE calculated from 3λ measured scattering. Once scattering was obtained at the 7λ, we estimated SSA and SSAAE at these 7λ.

a) The SAE depends on the physical properties of aerosols and mainly on the size of the particles. Generally, SAE lower than 1 or higher than 2 indicate that the scattering is dominated by larger or finer particles, respectively (Seinfeld and Pandis, 1998; Schuster et al., 2006). In this study SAE was estimated from a linear fit of 3λ scattering measured in the 450-635 nm range.

b) The *g* parameter (Delene and Ogren, 2002; Andrews et al., 2006) is defined as the cosine-weighted average of the phase function which is the probability of radiation being scattered in a given direction. Values of *g* can range from -1 for 180° backwards scattering to +1 for complete forward scattering (0°). A value of 0.7 is commonly used in radiative transfer models (Ogren et al., 2006).

c) The AAE provides information about the chemical composition of atmospheric aerosols. BC absorbs radiation in the whole solar spectrum with the same efficiency, thus it is characterized by AAE values around 1 (Kirchstetter et al., 2004; Kim et al., 2012). Conversely, BrC and mineral dust show strong light absorption in the blue to ultraviolet spectrum leading to AAE values up to 3 and 6.5 respectively (Kirchstetter, 2004; Chen and Bond, 2010; Kim et al., 2012; and Petzold et al., 2009). AAE was estimated from a linear fit of 7λ absorption measured in the 370-950 nm range.

d) The SSA parameter is defined as the ratio between the scattering and the extinction coefficients at a given wavelength and describes the relative importance of scattering and absorption on radiation. Thus the SSA parameter indicates the potential of aerosols for cooling or warming the atmosphere. A detailed description of SSA at both MSY and MSA was presented by Pandolfi et al., (2011) and (2014a), respectively. Nevertheless in this work the SSA is used with the main objective of calculating SSAAE.

e) The wavelength dependence of the SSA is known as the SSAAE and it is defined as SSAAE=(1-SSA)*(SAE-AAE) (Moosmüller and Chakrabarty, 2011). This parameter provides general information about the type of sampled aerosols integrating both physical and chemical properties, and it has been proposed as a good indicator for the

presence of Saharan dust in the atmosphere (Collaud Coen et al., 2004). The Saharan dust outbreaks change the intensive optical properties of sampled aerosols causing a reduction of SAE and an increase of AAE, resulting in a negative SSAAE during these events. Therefore this parameter can be used to assess which type of aerosol is dominating the scattering and the absorption. For example Collaud Coen et al. (2004) reported measurements performed at the high altitude alpine station Jungfraujoch (Switzerland) and showed that the SSAAE was able to detect 100% of Saharan dust outbreaks compared with 80% and around 40% of events detected using SAE and AAE, respectively. Russell et al. (2010) has also performed the AAE and SSAAE parameters for full aerosol vertical columns obtained from sun-sky photometer retrievals, in order to characterize aerosol columns dominated by the two important sources of UV absorbing aerosols, biomass burning and Saharan dust. ~~Other works have used SSAAE to distinguish between the two important sources of UV absorbing aerosols, biomass burning and Saharan dust, as is detailed in (Russell et al., 2010).~~ The SSAAE was estimated from a linear fit of 7λ-SSA calculated in the 370-950 nm range (Table 1).

4. The Aethalometer model

The Aethalometer (AE) model allows the detection of fossil fuel combustion (FF) and biomass burning (BB) contributions to the total BC concentrations taking advantage of the different spectral absorption efficiency of the main markers of these two sources: BC for FF combustion and BrC for BB (Sandradewi et al., 2008b). The AE model has also been applied for FF and BB source apportionment to total carbonaceous material (CM_{total}=OM+BC) and to organic matter (OM) (Favez et al., 2010). Light absorption measurements at 370-450 nm and 880-950 nm are used due to the fact that BC from FF combustion has a weak dependence on wavelength whereas BrC from BB shows enhanced absorption at shorter wavelengths. Here we applied the AE model to absorption measurements performed at 370 nm and 950 nm.

The AE model is usually applied selecting AAE values around 0.8-1.1 for BC from FF combustion (AAE_{ff}) and around 1.6-2.2 for BB (AAE_{bb}). It is known that the AE method may lead to high uncertainties in the estimation of biomass burning contribution due to the high variability of AAE_{bb} depending on the wood burned combustion regime and on the internal mixing with non-absorbing materials (Lewis et al., 2008; Harrison et al., 2013). Thus, AAE_{ff} and AAE_{bb} are usually chosen by comparing the AE model outputs with FF and BB contributions to BC and/or OM from other techniques such as chemical mass balance (CMB) model on off-line filter measurements, positive matrix factorization (PMF) model on AMS and/or ACSM data or ^{14}C technique (Favez et al., 2010; Herich et al., 2011; Crippa et al., 2013). Here we followed a similar procedure to calibrate the AE model: the optimal AAE_{ff} and AAE_{bb} were selected comparing results from the AE model with those obtained from PMF on simultaneous ACSM hourly data at MSY station for 1 year (Minguillón et al., 2015). Then, the optimal AAE_{ff} and AAE_{bb} for MSY were applied to MSA Aethalometer model.

In the present~~this~~ work, CM_{total} was calculated as the sum of BC concentration measured by MAAP (637 nm) and OM measured by ACSM. Following equations (1-3), CM_{total} was expressed as the sum of carbonaceous material from FF combustion (CM_{ff}), carbonaceous material from BB emissions (CM_{bb}) and non-combustion organic aerosols (OA). At MSY station, OA may account for a large contribution mainly in summer and includes principally organic aerosols from biogenic origin as reported in Minguillón et al. (2011) and Pandolfi et al. (2014b). Thus, we included the constant C_3 in contrast to previous studies where it was negligible assuming a low contribution of OA sources. CM_{ff} and CM_{bb} were then expressed as the product of the constants (C_1 and C_2) multiplied by the aerosol absorption due to FF at 950 nm ($b_{abs,ff,950}$) and the aerosol absorption due to BB at 370 nm ($b_{abs,bb,370}$), respectively. The $b_{abs,ff,950}$ and $b_{abs,bb,370}$ were calculated for different values of AAE_{ff} and AAE_{bb} following the equations reported in Sandradewi et al. (2008b) and then used in eqs. 1-3 for OM source apportionment. Finally, the constants C_1, C_2 and C_3, which related the light absorption to the particulate mass, were calculated by multilinear regression (MLR) analysis.

6

$$CM_{total} = CM_{ff} + CM_{bb} + OA \qquad (1)$$

$$OM + BC = C_1.b_{abs,ff,950} + C_2.b_{abs,bb,370} + C_3 \qquad (2)$$

$$OM + BC = (OM_{ff}+BC_{ff})_{950} + (OM_{bb}+BC_{bb})_{370} + OA \qquad (3)$$

Once BC_{ff}, BC_{bb}, CM_{ff} and CM_{bb} have been estimated, the contributions of FF and BB to OM (OM_{ff} and OM_{bb}) can be
calculated by subtracting BC to CM (Favez et al., 2010).

5. Results and discussion

5.1 General features

Mean, standard deviation, median, minimum, maximum, skewness and percentiles (5, 25, 50, 75, 95) of hourly extensive and
intensive aerosol optical properties used in this work are reported in Tables S2~~1a and S1b~~ for MSY and MSA. Although the
periods considered at the two stations were different, time coverage was sufficiently large to allow for a characterization of
the mean aerosol optical properties at the two sites. Mean values of scattering, backscattering and PM_{10} concentrations at
both sites were consistent with previous studies performed at these stations (Pandolfi et al., 2011, 2014a; Ripoll et al., 2014,
2015b). Higher σ_{sp} and σ_{bsp} were on average measured at MSY consistent with higher PM_{10} concentrations due to the larger
impact of anthropogenic sources at this station. Consequently, larger absorption σ_{ap} (Mm^{-1}) at 470 and 880 nm was also
observed at MSY (7.66±6.5 and 3.51±2.99) compared to MSA (3.57±3.95 and 1.59±1.71).

Mean values of g (525 nm), SAE and AAE at MSY station were 0.59±0.06; 1.38±0.79 and 1.30±0.30, respectively. At MSA
station mean values for these parameters were 0.57±0.14, 1.58±0.83 and 1.36±0.27. Mean SAE was higher at MSA station
compared to MSY which could be explained by a dominance of smaller particles on average at MSA likely due to frequent
position of the station within the free troposphere in winter. As already reported (Andrews et al., 2011; Berkowitz et al.,
2011; Marcq et al., 2010; Pandolfi et al., 2014a), under low aerosol loadings at mountain top sites ~~the aerosol mixture is
preferentially composed of relatively smaller (and darker) particles.~~, in which large aerosols scattering particles have been
preferentially removed, the aerosol mixture is mainly composed of relatively smaller and darker particles. Previous studies at
MSA have described the free troposphere conditions, characterized by very low PM_1 concentrations (<1.5 μg m^{-3}), low
values of SSA (0.83) and g (0.43) parameter, and increasing SAE (Pandolfi et al., 2014a). MSY site presented slightly lower
AAE values compared to MSA, due to a major predominance of black carbon particles as a consequence of the proximity to
Barcelona urban area. SSA was slightly higher at MSA (0.85±0.08 and 0.82±0.3) compared to MSY (0.83±0.07 and
0.8±0.12) at 470 and 880 nm, respectively.

5.2 Detection of Saharan dust outbreaks using aerosol intensive optical properties

As already observed, SDE can be detected using optical properties measurements taking advantage of the changes that
mineral dust causes in the spectral dependence of aerosol scattering and absorption (Collaud Coen et al., 2004). In fact SDE
scenarios are characterized by a decrease of SAE, as a consequence of the predominance of coarse particles, and an increase
of AAE due to the enhanced absorption in the UV spectrum by mineral dust. The angstrom matrix is a useful tool to detect
periods dominated by SDE (Russell et al., 2010), it consist of a scatterplot made up by SAE parameter in the x-axis and AAE
parameter in the y-axis, providing information about aerosol size and composition, respectively. The scatterplot can be
colour coded and investigated by other parameters in order to further characterize the atmospheric aerosols. In our case the
matrix was colour coded by different air mass origin and by the coarse fraction contained within the PM_{10} (%PM_{1-10} in
PM_{10}), which was calculated as the difference between %PM_1 and %PM_{10} contained within the PM_{10} fraction. ~~Therefore, the
scatter plot between AAE and SAE (called Ångström matrix) is useful to detect periods dominated by SDE (Russell et al.,
2010). Here we calibrate, based on the available tools, the Ångström matrices for MSY and MSA in order to use them for
SDE detection.~~

The Ångström matrix for MSY and MSA (Fig. 2b, e) showed dominance of coarse material (high % of PM_{1-10} in PM_{10}) related to low values of SAE (roughly lower than 1) and larger values of AAE (approximately higher than 1.3) during SDE.

In order to demonstrate that these SAE and AAE limits were mainly related with the presence of mineral dust from Africa in the area under study, the Ångström matrices were also ~~weighted~~ investigated by the occurrence of the three main atmospheric situations~~scenarios~~ affecting MSY and MSA stations: SDE, REG and AA (Figs. 2a, d). As shown in Figs. 2a, d the region of the Ångström matrices representing SDE well fits with the SAE and AAE limits reported above (Figs. 2b, e). Average and standard deviation of SAE and AAE during SDE were 1.12±0.87 and 1.27±0.24 for MSY, and 0.69±0.78 and 1.41±0.25 for MSA. Lower SAE and higher AAE at MSA pointed to a larger dominance of mineral dust and a purer composition during these events at the high altitude station (Fig. S1). Average PM_{10} concentrations during SDE were 25.4±17 and 21.0±17 µg m^{-3} for MSY and MSA respectively. Further information providing the frequency distribution and average values of SAE, AAE, PM_{10} and %PM_{1-10} in PM_{10} for each atmospheric situation at both stations is reported in Fig. S1.

The feasibility of detecting Saharan dust outbreaks by means of the hourly Ångström matrices is further confirmed in Fig. S2~~1~~, where the Ångström matrix for MSY station was weighted by the %dust (daily base) for those days affected by SDE. The quantification of African mineral dust contribution to PM_{10} (%dust) at MSY was calculated by the statistical methodology described in Escudero et al. (2007b) and Pey et al. (2013a) (detailed in sub section 2.2). Despite the scarce availability of simultaneous daily data points of SAE, AAE and %dust for the period under study, the Ångström matrix showed lower SAE and increasing AAE with increasing intensity of SDE (%dust), in agreement with the Ångström matrix reported in Fig. 2b. However, Fig. S2~~1~~ clearly shows that there are conditions when the AAE-SAE pair does not unequivocally detect the Saharan dust outbreaks, being SAE higher than 1.0-1.5 and AAE lower than 1.2-1.3. These points are characterized by relatively low (<40% approximately) dust contribution to PM_{10} representing not very intense SDE. Thus, this region of the Ångström matrix identified an aerosol mixture between mineral dust and anthropogenic pollutants of mainly local origin. Then, we can conclude that: a) some points during REG episodes (yellow dots in Figs. 1a, d) were characterized by SAE and AAE values similar to those observed during SDE indicating presence of mineral dust in the atmosphere, and that b) for some SDE, the corresponding AAE-SAE pairs do not unequivocally confirm the presence of mineral dust (anthropogenic emissions and mineral dust mixing).

The blue spot area displayed in the Ångström matrix for MSA station (Fig. 2e) showed AAE-SAE pairs characterized by low contribution of PM_{1-10} to PM_{10}~%1-10, which are mainly represented by AA scenarios. Average and standard deviation of SAE and AAE during these scenarios were 1.35±0.95 and 1.33±0.27 for MSY, and 1.65±0.57 and 1.30±0.16 for MSA, respectively. PM_{10} showed the lowest concentrations during these events, being 11±7 and 9.4±6 µg m^{-3} respectively for MSY and MSA (Fig. S1). These AA scenarios, some of them related with free troposphere conditions in MSA during winter, lead to a cleaner environment free of pollutants characterized by finer and relatively darker particles in the Ångström matrix. Conversely, a predominance of REG scenarios is seen at MSY (yellow dots in Fig. 1a), related to larger contribution of PM_{1-10} to PM_{10} (40-80%) (Fig. 2b). SAE and AAE values during REG episodes were 1.61±0.87 and 1.24±0.19 for MSY, and 1.66±0.48 and 1.29±0.15 for MSA, respectively. The average PM_{10} concentrations during these atmospheric situations were 15.6±8 and 12.6±7 µg m^{-3}.for MSY and MSA (Fig. S1). REG episodes, mainly related to pollution scenarios, are characterized by local (affecting lower altitude regions driven by the breeze patterns) to regional (reaching higher altitude locations driven by larger circulations and upslope winds) atmospheric circulations transporting fine particles from the urbanized/industrialized coastline. ~~Mean~~ SAE ranged between ~~1.50~~-3 and 1.~~3~~-2.5~~3~~ at MSY and MSA stations, respectively, during REG scenarios, whereas main AAE values ranged between 1-1.7 at both stations. Recently, Mallet et al. (2013) reported column-integrated AAE (440-870 nm) values across the Mediterranean using Level 2 AERONET data varying from around 1.3 in urban areas to more than 2 at Mediterranean dusty sites.

In order to study how SDE affect the asymmetry parameter in the area under study, Figs. 2c and, f show a modified Ångström matrix where the g parameter was investigated instead of SAE at both stations. This parameter can also be used to estimate the size of aerosols according to the difference in the scattering direction presented by small and larger particles, since larger particles present higher forward than backward scattering. During SDE, g was similar at both stations, approximately ranging between 0.55-0.75 at MSA and between 0.5-0.7 at MSY. These results are in agreement with those g values reported by Ogren et al. (2006) for other in situ measurements. Therefore, given that SAE parameter presents larger variability than g in relation to changes in %PM$_{1-10}$, we conclude that SAE is a better proxy for estimating aerosol size. Despite this, providing experimental variability ranges for g is important given that the asymmetry parameter is commonly used in radiative transfer models (Ogren et al., 2006).

As already mentioned, the SSAAE has been identified as a good indicator for Saharan dust outbreaks at mountain top sites being negative during these types of events (Collaud Coen et al., 2004). The SSAAE is a useful parameter, which can be used together with the Ångström matrix in order to characterize mineral dust at different emplacements with the aim to identify SDE in real-time. Similarly to what already observed for the Ångström matrices, our results showed that the feasibility of detecting SDE by means of SSAAE depended on both the location and altitude of the measurement station, which determines the aerosol background concentration, and the intensity of the SDE.

Figure 3a showed a relationship between SSAAE and %dust at MSY for those days affected by SDE. At MSA, where %dust was not calculated due to limitations of the methodology, SSSAE did correlate with percentage of coarse particles in PM$_{10}$ (Fig. 3b). SSAAE became negative for most of the SDE identified at MSA accounting for 85% detection of these events. However SSAAE showed more frequently positive values near to zero at MSY, detecting 50% of SDE due to a larger exposure to anthropogenic emissions. The SSAAE became negative when the relative contribution of Saharan dust to PM$_{10}$ (%dust) at MSY was higher than approximately 60%, keeping positive values at lower %dust in PM$_{10}$ despite the presence of mineral dust.

Figure 3c shows an example of the daily variation of SSAAE, SAE and AAE at MSY during a SDE. Low values of SAE (<1) and higher values of AAE (>1.5) lead led to negative SSAAE during the night, indicating presence of mineral dust. Conversely, during the day, anthropogenic fine pollutants transported from nearby polluted areas hindered the optical effect of mineral dust during non-intense SDE (54% of dust in PM$_{10}$). Consequently, despite the impact of mineral dust, the SSAAE turned into positive values. SAE reached values around 2 indicating dominance of fine particles and, correspondingly, the AAE lowered to around 1.2 indicative that these fine particles were mainly of anthropogenic origin. Thus, the proximity to anthropogenic sources under specific atmospheric conditions (i.e. strong breeze and low SDE intensity) can prevent both the Ångström matrix and the SSAAE parameter from detecting SDE.

A different scenario is shown in Fig. 3d, where two Saharan dust outbreaks were detected and highlighted by the yellow rectangles. The SSAAE was negative during the two outbreaks keeping negative values between the two events despite the influence of Atlantic air masses during the days 23th and 24th October 2013. Interestingly, the SSAAE reached the lowest negative values during the subsequent days after the SDE, until precipitation scavenged pollutants from the atmosphere (highlighted by the blue rectangle). Thus, the local and regional recirculation of air masses under the REG episode, often lasting for a few days, recirculated an aerosol mixture dominated by coarse Saharan particles in the atmosphere at a level able to cause the SSAAE be negative even in absence of African air mass advection (Fig. S3₂). It is interesting to highlight that despite the intensive optical parameters showed the presence of mineral dust during the REG episode, with SSAAE<0 and the corresponding decreasing SAE and increasing AAE, the Dream was not able to reproduce the recirculation of mineral dust (Fig. S3d), and only a simulation at high spatial resolution could characterize the event. The evidence that mineral dust can recirculate under dry conditions in summer for a few days after the SDE is of high relevance for air quality. Thus, near-real-time aerosol optical parameters such as SSAAE are very useful to detect mineral dust in the atmosphere even after the end of the event.

9

5.3 Detection of biomass burning using aerosol optical properties

5.3.1 Calculation of the constants from the Aethalometer model

In order to test the stability of the AE model for our emplacement (MSY), C_1, C_2 and C_3 were calculated varying (Table 2): a) AAE_{bb} between 1.8 and 2.2 (for a fixed $AAE_{ff}=1$), and b) AAE_{ff} between 0.9 and 1.1 (for a fixed $AAE_{bb}=2$). In the first case (a) C_1 showed a very low variability keeping values around 1.05 ± 0.01 g m^{-2} ,whereas C_2 showed a higher variability ranging between 0.28 g m^{-2} ($AAE_{bb}=1.8$) to 0.24 g m^{-2} ($AAE_{bb}=2.2$). In our work C_3, which represents the contribution from non-combustion OM, was estimated in around 0.31 ± 0.04 µg m^{-3}. These results were consistent with previous studies dealing with AE source apportionment to OM and reporting less variability for C_1 compared to C_2 (Sandradewi et al., 2008b; Favez et al., 2010). In another study (Herich et al., 2011) the AE model was not applied to OM mainly due to the high variability (i.e. model instability) observed for C_1 from different model outputs. In the second case (b), C_1 changed only little (less than 10%) ranging between 1.01 g m^{-2} ($AAE_{ff}=0.9$) to 1.09 g m^{-2} ($AAE_{ff}=1.1$) for a fixed AAE_{bb} of 2. As reported below, AAE_{bb} for our environment was set to 2 by comparison with ancillary experimental measurements, whereas AAE_{ff} was set to 1 as in previous studies, given the lower sensitivity of the AE model to AAE_{ff} compared to AAE_{bb}. It is important to consider that the values of C_1 (~1.05 g m^{-2}) and C_2 (~0.26 g m^{-2}) calculated for our emplacement were different from those reported in previous studies for different environments. In their works, Favez et al. (2010; Grenoble) and Sandradewi et al. (2008b; Roveredo, Switzerland) set C_1 to a fixed value of 0.26 g m^{-2}, being this parameter less variable, and C_2 was estimated around 0.7-0.8 g m^{-2}. Differences between the constants were due to the larger use of biofuel for domestic heating in these later locations, leading to higher contribution of BB to BC compared to FF combustion sources (and probably less effect of FF sources). Contrary to our emplacement where results indicated (as shown later) higher contribution from FF sources compared to BB for both BC and OM.

Given the large differences our constants C_1 and C_2 showed compared to previous studies for different environments, we applied here a similar procedure as described in Herich et al. (2011). Thus, we simulated CM_{total} using C_1 and C_2 from Sandradewi et al. (2008b) and Favez et al. (2010), and $b_{abs,ff,(\lambda1)}$ and $b_{abs,bb,(\lambda2)}$ as derived from our measurements. As expected the results showed very low correlation between calculated and measured CM ($R^2=0.009$; slope=0.65) compared to $R^2=1$ and slope=1 using our calculated constants C_1, C_2 and C_3. Therefore we conclude that calculation of the specific constants of the model for the area under study is required in order to successfully perform the Aethalometer model.

Moreover, we calculated C_1, C_2 and C_3 for two more different cases: (a) including only the winter season in order to account for a larger contribution of BB emissions and to reduce the influence of non-combustion OM and SOA formation which maximize in summer at MSY station (Minguillón et al., 2011), and (b) excluding SDE from the database which could overlap with BrC being both, BB and mineral dust, important absorbers in the UV. The differences for C_1, C_2 and C_3 calculated between these two cases and the whole period (June 2012–July 2013, Table 2) in case (a) were lower than 10%, 20% and 15%, respectively. These differences were around 3%, 6% and 34%, respectively, for the case (b). Given that the AE model outputs have been estimated having errors as high as 50% (Favez et al., 2010) and given that we are continuously measuring absorption with the AE instrument at MSY and MSA without ACSM data, the model was calibrated using 1 year data set in order to apply the AE model at any other period without ancillary measurements.

5.3.2 Validation of the Aethalometer model with simultaneous experimental data

Very few studies have been published comparing outputs from the AE model with the source apportionment of the ACSM measurements (Favez et al., 2010). Biomass burning organic aerosol (BBOA) and hydrocarbon-like organic aerosol (HOA) from ACSM data refer to primary organic aerosols (POA) whereas OM_{bb} and OM_{ff} from AE model include SOA formed from these primary sources. Since simultaneous measurements to the study period were not deployed for differentiating POA to SOA ratios, we have considered results previously reported for MSY. SOA formation from biomass burning emissions can be up to 25% of the BBOA emitted, as shown by Cubison et al. (2011) using Aerosol Mass Spectrometer (HR-ToF-

AMS) data. This ratio was primarily applied by Minguillón et al. (2015) to the results obtained from the source apportionment to ACSM performed at MSY station, which were also used in this study. Moreover, based on the results from the DAURE campaign carried out in March 2009 at MSY station, the organic carbon (OC) originated from fossil sources is only 15% primary at MSY (Minguillón et al., 2011), which corresponds to 10% if OM is considered instead of OC. Thus, we assume that primary BBOA and HOA represent approximately 75% and 10% of the OM_{bb} and OM_{ff}, respectively, at MSY station.

Relationships between BBOA and OM_{bb} concentration for different AAE_{bb} values (Table 3) showed good agreement ($R^2 \sim 0.43$) with slopes ranging between 1.1 and 2.2 depending on the AAE_{bb} used. The relationship between OM_{ff} and HOA showed less variable slope (F) (around 4) but more variable R^2 between 0.43 and 0.63. Choosing $AAE_{bb}=2$ and $AAE_{ff}=1$ we obtained: a) an OM_{bb}/BBOA ratio of around 1.27 ($R^2=0.43$) in agreement with 25% of SOA formation from primary biomass burning emissions estimated by Cubison et al. (2011); and b) an OM_{ff}/HOA ratio of 4.4 ($R^2=0.6$) which is consistent with 90% portion of SOA found at MSY in previous studies (Minguillón et al., 2011). The correlations were only moderate mainly due to the variable SOA formation, which is partially driven by the environmental conditions, as opposed to the primary OA emissions. Moreover, it should be noted that the slopes and R^2 in Table 3 were obtained using hourly averages. Scatterplots by bins (Fig 4) showed that the relationships had slopes in agreement with those reported in Table 3 but much higher R^2 (0.97).

The relationship between OM_{bb} and BBOA calculated only for the winter period using hourly data showed $R^2=0.4$ and F=0.96. The slope was close to the unity due: to the lower SOA formation in winter, mainly explained by a decreasing of VOCs emissions being one of the primarily precursor sources of SOA formation during the warmer period in this emplacement (Seco et al.,), and also as consequence of less photochemistry activity and the prevalence of primary emissions. ~~The slope was close to the unity due to the lower SOA formation in winter, consequence of less photochemistry activity, and the prevalence of primary emissions.~~ Experimental measurements of Nitrogen dioxide (NO_2), which is mainly related to fossil fuel emissions, agrees well ($R^2=0.64$) with BC_{ff} obtained from $AAE_{bb}=2$ and $AAE_{ff}=1$ for the winter period at MSY (Fig. 5).

Besides uncertainties in determining FF and BB contributions from the Aethalometer model, results from sensitivity test analysis showed good agreement with experimental measurements and good stability of the model. We have shown that the constants C_1, C_2 and C_3 depend on the relative contributions of FF and BB, thus these constants are site-dependent and should be calculated for each measurement emplacement. Moreover, a calibration of the model is necessary to determine the most suitable AAE_{ff} and AAE_{bb} pair for a reliable estimation of fossil fuel and biomass burning contributions. Interestingly AAE_{bb} and AAE_{ff} chosen in this work were the same as in other studies, suggesting a stable value of AAE=2 for characterizing BB emissions within the model. Our results showed that the higher AAE_{bb} the lower the estimated BC_{bb} contribution, which ranged between 35-45% depending on the AAE_{bb} used (1.8-2.2).

5.3.3 Seasonal and daily variation of fossil fuel and biomass burning contribution to BC and OM at MSY and MSA stations

Seasonal and daily AAE and relative contributions of BB and FF to BC (at both MSY and MSA) and to OM (at MSY only) from the Aethalometer model are shown in Fig. 6. Both environments are characterized by similar average PM chemical composition (Ripoll et al., 2015b), thus probably leading to similar mean values of AAE at MSY (1.30±0.30) and MSA (1.36±0.26) (Figs. 6a, e). Thus, AAE_{ff} and AAE_{bb} determined for MSY were used also for MSA.

MSY showed slightly lower AAE as a consequence of higher exposure to FF emissions sources compared to MSA. AAE at MSA and MSY showed larger values on average in winter suggesting a higher contribution of BrC. AAE monthly averages reached around 1.5 at both sites. Despite the fact that the lowest BC and OM concentrations were observed in winter the AAE showed the highest values indicating larger contribution of BB sources at both stations. It is interesting to note that on average AAE was higher at MSY than at MSA during winter months (December-January) suggesting higher relative BB

contribution at MSY compared to MSA in winter (Fig. 6e and S43a). This was likely due to the fact that MSA station is often above the polluted PBL in winter whereas MSY, located at lower altitude, is usually within the PBL and frequently affected by local pollutants accumulated under winter anticyclonic conditions (Pandolfi et al., 2014b; Ripoll et al., 2015b). Low values of AAE during the day and higher at night at both sites resulted mainly from the development of sea and mountain breezes, favouring the transport of anthropogenic pollutants from the urbanized/industrialized coastline and valleys to inland areas and leading to an increase of AAE during the warmest hours of the day (Fig. 6a).

The measured BC was well reproduced by the sum of BC_{ff} and BC_{bb} contributions from the AE model showing slightly overestimation, by 11% and 15% at MSY (Fig. 6c, g) and MSA (Fig. 6d, h), respectively, on annual average. However, measured OM is underestimated by the sum of OM_{ff} and OM_{bb} at MSY, due to the large contribution of carbonaceous material from non-combustion sources (C_3) during the warmer months (27%) (Fig. 6f). This difference was mainly driven by biogenic sources which are expected to have important contribution in our measurement emplacement, particularly in summer due to the SOA formation. Then C_3 time variation was well reproduced by the model showing larger contribution during the summer period. Nevertheless, based on the available previous studies performed at MSY (Minguillón et al., 2011 and 2015; Pandolfi et al., 2014b), C_3 contribution might be slightly underestimated due to possible apportionment within OM_{ff} and/or OM_{bb}. It should also be noted that some SOA UV absorbing compounds originated from anthropogenic sources, such as nitroaromatic compounds which are the major contributors to the light absorption of the toluene SOA (Laskin et al., 2015), may be partially apportioned within OM_{bb}, possibly resulting in an overestimation of this later.

Interestingly, a relationship was observed between AAE and the relative contribution of BC_{bb} to BC concentrations at MSY and MSA (Fig. 7). AAE increased up to 1.5 when $\%BC_{bb}$ was higher than around 50% of the total measured BC. The intercept of the linear fit was 1.01 and 1.15 at MSY and MSA, respectively, pointing to BC from FF sources as main absorber in absence of biomass burning events. Therefore, we can clearly appreciate the effect of BrC from biomass burning on AAE even if the mean BC_{bb} contributions (0.13 µg m^{-3} and 0.06 µg m^{-3}) at MSY and MSA, respectively, to the total BC were quite low (36% and 40%). Mean OM_{bb} concentration at MSY was 0.9 µg m^{-3}, accounting for a 30% contribution to total OM.

The prominent increase of FF contribution at MSY and MSA in summer, when both stations are within the PBL and dominated by similar atmospheric circulations, is in agreement with lower AAE values. Stronger summer recirculation processes which are strengthened by sea and mountain breezes favour the transport of pollutants toward regional areas inland. Daily variation of both BC and OM is mainly driven by FF combustion from Barcelona anthropogenic sources. The daily cycle is more pronounced at MSY as a consequence of the proximity to Barcelona Metropolitan Area and the lower altitude compared to MSA. Despite OM is mainly driven by biogenic sources during the summer period at MSY, significant FF contribution is registered during the warmest hours of the day (Fig. S43b). However BB sources time variation, from both BC and OM, are led by local atmospheric processes as domestic heating turning into a dominant source during the colder months at both stations. Thus, during winter, BC_{bb} and BC_{ff} showed almost the same contribution reaching the maximum values in the afternoon (Fig. S43c). Conversely OM_{ff} daily cycle is decoupled from OM_{bb}, showing this later larger concentrations during the night given that it is mainly led by BB emissions from domestic heating emitted during the colder hours, and also possibly as a result of SOA formation after the OM was emitted (Fig. S43b). Note that during the night OM_{bb} concentration does not present large variations, possibly because it remains as a residual layer above the thermal inversion.

FF contribution to OM and BC was found to be significant at MSY, according to the large values obtained for C_1 constant in the Aethalometer model. In order to compare the results with different source apportionment methods, the fossil fuel and non-fossil fuel contribution to EC (EC_{ff}, EC_{non_ff}) and OC (OC_{ff}, OC_{non_ff}) reported by Minguillón et al. (2011) by means of the ^{14}C technique at MSY for the periods February-March and July 2009 were taken as a reference. Given that AE measurements were not available at MSY during those periods, we averaged available contributions from the Aethalometer model for the same time-of-the-year periods during 2012, 2013 and 2014 for BC and during 2012 for OM. Despite the lack

of overlapping in the dataset, results for BC contributions from both techniques (^{14}C and AE model) showed good agreement. BC_{ff} contributions calculated by the AE model in winter and summer were 53% and 73% respectively, whereas EC_{ff} contributions derived from ^{14}C measurements accounted for 66% and 79%. However larger discrepancies were found for FF and BB contributions to OM. Results from the ^{14}C technique identified a FF contribution to OC of 31% and 25% for winter and summer, respectively, whereas the AE model resulted in a OM_{ff} contribution of 39% and 58%, respectively. We also saw a OM_{bb} contribution around twice more than OC non-fossil fuel. The apparently overestimation of OM_{bb} and OM_{ff}, particularly in summer, compared to the available results from ^{14}C might be possibly led by the partially apportionment of non-combustion carbonaceous material and SOA anthropogenic within OM_{bb} and/or OM_{ff}, as we commented above.

A second assessment of the AE model results was carried out by comparison with OA source apportionment results reported by Minguillón et al. (2015) for winter (28 October-7 April 2013) and summer (14 Juny-9 October 2012) at MSY based on ACSM measurements. The agreement needs to be evaluated considering the different outputs from each method; thus whereas the ACSM OA source apportionment identifies the contribution of primary fossil fuel (HOA) and biomass burning (BBOA) contributions, the AE model calculates the total (including the SOA) fossil fuel (OM_{ff}) and biomass burning (OM_{bb}) contributions. HOA contribution was 12% and 13% for winter and summer, whereas OM_{ff} accounted for 47% and 59%. BBOA was identified only in winter with a contribution of 28%, and OM_{bb} contribution was 37% for the same period. These results are in agreement assuming the ratios OM_{ff}-to-HOA and OM_{bb}-to-BBOA based on SOA-to-POA proportion, used in the previous section 5.4.3 in order to calibrate the Aethalometer model and fit the most suitable AAE_{ff} and AAE_{bb} representative of our environment.

An interesting wildfire episode detected at MSY took place the 23th of July 2012 with AAE increasing significantly up to 2 and the lowest value at 1.3 (Fig. 8). BB sources dominated BC and OM contributions accounting for 73% and 78% respectively, until the breezes were developed and transported pollutants from urban areas toward the station during the warmest hours of the day, resulting in a decrease of the AAE. As we shown previously for the whole dataset, good agreement was found between measured and simulated BC. Conversely OM was slightly underestimated during the sunlight hours likely due to biogenic emissions and SOA formation by photochemical reactions.

The concomitance of biomass burning and wildfire episodes during SDE may be an issue, being both dust and BB strong absorbers in the UV. The SAE is a useful parameter that should be considered in order to establish differences in near real-time between mineral dust (coarse material) and biomass burning (finer aerosol). However, since relatively low BB concentration was found in the area under study, the dominance of mineral dust appears to be larger with respect to BB regarding the effects on intensive optical properties. Furthermore the co-occurrence of SDE and BB winter emissions is not usual. Whereas for differentiating wildfires episodes and SDE, both frequently occurring during summer, wildfires can be considered as isolated events and detected by means of different tools such as back-trajectories, forecast models and remote sensing data.

6. Conclusions

The present work shows the variations of the intensive aerosol optical properties measured at regional (Montseny) and continental (Montsec) background stations in the WMB. We have studied the feasibility of using the near real-time optical measurements performed at these stations for the detection of specific atmospheric pollution episodes affecting the WMB: Saharan dust and biomass burning.

The Ångström matrix revealed that Saharan dust events (SDE) in the WMB were characterized by SAE on average lower than 1 due to the larger size of mineral dust particles and AAE values higher than 1.3 (up to 2.5 depending on the intensity of SDE) indicating absorption in the UV by iron oxide contained within the mineral dust. Linear relationships were found between AAE and increasing %dust at MSY (0.7) and $\%PM_{1-10}$ at MSA (0.4) confirming the enhanced absorption in the UV

due to mineral dust from SDE. Interestingly, SAE showed higher sensitivity than g to characterize the size of aerosols, ranging this latter between 0.55-0.75 and 0.50-0.70 at MSY and MSA respectively during SDE.

Feasibility of detecting SDE by means of SSAAE depended on both the location and altitude of the measurement station, which determines the aerosol background concentration, and the intensity of the SDE. Better results were shown at higher altitude locations, at MSA were detected most of the SDE (85%), whereas at MSY, with a larger exposure to anthropogenic pollutants, the detection of SDE depended mainly on the intensity of the Saharan dust outbreak. At MSY site 50% of SDE were detected, which were unequivocally identified when the relative contribution of mineral dust to PM_{10} was higher than 60%.

The proximity to anthropogenic sources of mainly fine particles can prevent both the Ångström matrix and the SSAAE parameter from detecting SDE. We have shown that transport of anthropogenic pollutants (mainly finer particles and precursors) from the urbanized/industrialized coastline towards regional areas inland can hinder the effect of mineral dust on the intensive aerosol optical properties during less intense SDE. We have also shown that regional atmospheric ~~circulations~~ scenarios occurring after SDE may favour the ~~resuspension~~ recirculation of mineral dust at regional level in the WMB. Thus mineral dust can remain in the atmosphere for a few days after the SDE. This fact is highly relevant for air quality since SDE frequently promote exceedances in the PM_{10} daily limit value.

Thus, depending on the background atmospheric conditions, not all SDE can be clearly detected using SAE, AAE and SSAAE parameters. And then additional information provided i.e. by forecast models, back trajectories analysis, and columnar measurements is also required in order to better detect and characterize these events. Nevertheless, aethalometer and nephelometer instruments provide near real time measurements and allow a fast detection of the impact of SDE at ground level. Furthermore, due to the sensitiveness for detecting changes in aerosol size and composition, SSAAE and Angstrom matrix tools are more sensitive compared to other near real-time measurements.

A sensitivity test performed to the Aethalometer model at MSY showed that the model constants, which are representative of the main emission sources, are actually site-dependent and should be calculated for the area under study. FF sources showed larger contribution than BB at MSY, leading to C_1=1.05 and C_2=0.26 (g m^{-2}) for AAE_{ff}=1 and AAE_{bb}=2. Moreover C_3 was found to be significant mainly due to the large contribution of biogenic sources at MSY, showing values around 0.31 (µg m^{-3}). Linear relations were found for comparisons between OM_{bb} vs. BBOA (R^2=0.43) and OM_{ff} vs. HOA (R^2=0.6) showing fitting slopes of 1.27 and 4.4 respectively, which are consistent with SOA formation from BB and FF (25% and 90%) emissions. Results from these comparisons were used in order to calibrate the Aethalometer model, pointing to AAE_{bb}=2 and AAE_{ff}=1 as the most suitable values for our emplacement.

Annual averages of BC_{bb} contributions at MSY (36%) and MSA (40%) were significantly lower compared to other studies in northern Europe, due to a lesser use of biomass burning as heating system. OM_{bb} contributions accounted for 30%. BB source contribution to both BC and OM were predominant during winter, with increasing AAE up to 1.5 when $\%BC_{bb}$ was higher than 50%. Nevertheless, BC and OM were ~~leaded~~led by FF emissions sources during the summer period, due to stronger summer recirculation processes which are strengthened by sea and mountain breezes favouring the transport of pollutants toward regional areas inland. An interesting wildfire episode showed AAE values up to 2, accounting for BB contributions to BC and OM of 73% and 78% respectively.

The Aethalometer model is a powerful tool to reproduce long periods of real-time FF and BB contribution to BC, even in those areas where there is a predominance of carbonaceous material from non-combustion sources and BB emissions does not present very large contributions. BC, as the sum of BC_{ff} and BC_{bb}, was well reproduced showing a slightly overestimation of 11% and 13% at MSY and MSA. Results for BC_{ff} and BC_{bb} in winter and summer were in agreement with previous studies at MSY deployed by ^{14}C analysis. Furthermore BC_{ff} and NO_2, both representative of traffic sources, showed good correlation for the winter period (R^2=0.64).

However, the model presents larger uncertainty concerning OM apportionment as reported in other studies (Favez et al., 2010; Herich et al., 2011). Biogenic sources, which present important contribution in our emplacement, are probably slightly underestimated by the model due to the partially apportionment of C_3 constant within OM_{ff} and OM_{bb}. Furthermore OM_{bb} might be slightly overestimated due to the account of anthropogenic SOA within it, which can overlap the absorption in the UV range. Despite the uncertainties associated to the source apportionment technique, OM time variation appears to be well reproduced. Nevertheless, ~~it should be taken into account~~ OM formation and transformation processes occurring in the NWM should be taken into account at the time of performing the AE model results, where important photochemical reactions take place ~~leaded~~led by large anthropogenic emissions and high insolation (mainly in summer). ~~Then, further research is needed in the identification of BrC emissions sources and their effects on optical properties, in particular for SOA formation and transformation processes.~~

The differentiation of brown carbon originated from different emission sources by using optical measurements is a challenge, in particular the SOA formation and transformation processes. Due to the uncertainties presented by the aethalometer model for providing absolute concentrations, it is recommended to carry out simultaneous measurements/experiments applying different techniques not based on optical methods, such as using levoglucosan as BB tracer or calibrating the model with BBOA obtained from ACSM source apportionment, in order to assess the quantification of biomass burning by the model. Nevertheless, the aethalometer model is a very useful tool which provides satisfactory estimations of the temporal variability of the contributions for both, biomass burning and fossil fuel emission sources. And then further research in characterizing brown carbon by means of optical techniques is needed in order to exploit the possibilities of the instrument.

The nephelometer and aethalometer instruments are widely used within monitoring networks and present several advantages for near real-time air quality monitoring at high temporal resolution. We have demonstrated the potential of ~~in situ aerosol optical measurements~~the intensive optical parameters obtained from both instruments for detecting specific air pollution scenarios in near real-time. This is possible given the high sensitivity of particular intensive aerosol optical parameters to characterize different types of atmospheric aerosols. However, it is necessary to perform a previous sensitivity test in order to evaluate and calibrate the intensive optical properties for detecting specific pollution episodes at different emplacements.

References

Alastuey, A., Minguillón, M. C., Pérez, N., Querol, X., Viana, M., and de Leeuw, F.: PM10 measurement methods and correction factors: 2009 status report, ETC/ACM Technical Paper 2011/21, 2011.

Albrecht, B. A.: Aerosols, Cloud Microphysics, and Fractional Cloudiness, Science, 245(4923), 1227–1230, doi:10.1126/science.245.4923.1227, 1989.

Alfaro, S. C., Lafon, S., Rajot, J. L., Formenti, P., Gaudichet, A. and Maillé, M.: Iron oxides and light absorption by pure desert dust: An experimental study, J. Geophys. Res., 109(D8), D08208, doi:10.1029/2003JD004374, 2004.

Andreae, M. O. and Gelencsér, A.: Black carbon or brown carbon? The nature of light-absorbing carbonaceous aerosols, Atmos. Chem. Phys., 6(10), 3131–3148, doi:10.5194/acp-6-3131-2006, 2006.

5 Andrews, E., Sheridan, P. J., Fiebig, M., McComiskey, A., Ogren, J. A., Arnott, P., Covert, D., Elleman, R., Gasparini, R., Collins, D., Jonsson, H., Schmid, B. and Wang, J.: Comparison of methods for deriving aerosol asymmetry parameter, J. Geophys. Res., 111(D5), D05S04, doi:10.1029/2004JD005734, 2006.

Andrews, E., Ogren, J. A., Bonasoni, P., Marinoni, A., Cuevas, E., Rodríguez, S., Sun, J. Y., Jaffe, D. A., Fischer, E. V., Baltensperger, U., Weingartner, E., Coen, M. C., Sharma, S., Macdonald, A. M., Leaitch, W. R., Lin, N.-H., Laj, P., Arsov,

10 T., Kalapov, I., Jefferson, A. and Sheridan, P.: Climatology of aerosol radiative properties in the free troposphere, Atmos. Res., 102(4), 365–393, doi:10.1016/j.atmosres.2011.08.017, 2011.

Basart, S., Pérez, C., Nickovic, S., Cuevas, E. and Baldasano, J. M.: Development and evaluation of the BSC-DREAM8b dust regional model over Northern Africa, the Mediterranean and the Middle East, Tellus B, 64(1), doi:10.3402/tellusb.v64i0.18539, 2012.

15 Berkowitz, C. M., Berg, L. K., Yu, X.-Y., Alexander, M. L., Laskin, A., Zaveri, R. A., Jobson, B. T., Andrews, E. and Ogren, J. A.: The influence of fog and airmass history on aerosol optical, physical and chemical properties at Pt. Reyes National Seashore, Atmos. Environ., 45(15), 2559–2568, doi:10.1016/j.atmosenv.2011.02.016, 2011.

Bond, T. C., Doherty, S. J., Fahey, D. W., Forster, P. M., Berntsen, T., Deangelo, B. J., Flanner, M. G., Ghan, S., Kärcher, B., Koch, D., Kinne, S., Kondo, Y., Quinn, P. K., Sarofim, M. C., Schultz, M. G., Schulz, M., Venkataraman, C., Zhang, H.,

20 Zhang, S., Bellouin, N., Guttikunda, S. K., Hopke, P. K., Jacobson, M. Z., Kaiser, J. W., Klimont, Z., Lohmann, U., Schwarz, J. P., Shindell, D., Storelvmo, T., Warren, S. G. and Zender, C. S.: Bounding the role of black carbon in the climate system: A scientific assessment, J. Geophys. Res. Atmos., 118(11), 5380–5552, doi:10.1002/jgrd.50171, 2013.

Chen, Y. and Bond, T. C.: Light absorption by organic carbon from wood combustion, Atmos. Chem. Phys., 10(4), 1773–1787, doi:10.5194/acp-10-1773-2010, 2010.

25 Collaud Coen, M., Weingartner, E., Schaub, D., Hueglin, C., Corrigan, C., Henning, S., Schwikowski, M. and Baltensperger, U.: Saharan dust events at the Jungfraujoch: detection by wavelength dependence of the single scattering albedo and first climatology analysis, Atmos. Chem. Phys., 4(11/12), 2465–2480, doi:10.5194/acp-4-2465-2004, 2004.

Collaud Coen, M., Weingartner, E., Apituley, A., Ceburnis, D., Fierz-Schmidhauser, R., Flentje, H., Henzing, J. S., Jennings, S. G., Moerman, M., Petzold, A., Schmid, O., and Baltensperger, U.: Minimizing light absorption measurement artifacts of

30 the Aethalometer: evaluation of five correction algorithms, Atmos. Meas. Tech., 3, 457-474, doi:10.5194/amt-3-457-2010, 2010.

Crippa, M., DeCarlo, P. F., Slowik, J. G., Mohr, C., Heringa, M. F., Chirico, R., Poulain, L., Freutel, F., Sciare, J., Cozic, J., Di Marco, C. F., Elsasser, M., Nicolas, J. B., Marchand, N., Abidi, E., Wiedensohler, A., Drewnick, F., Schneider, J., Borrmann, S., Nemitz, E., Zimmermann, R., Jaffrezo, J.-L., Prévôt, A. S. H. and Baltensperger, U.: Wintertime aerosol

35 chemical composition and source apportionment of the organic fraction in the metropolitan area of Paris, Atmos. Chem. Phys., 13(2), 961–981, doi:10.5194/acp-13-961-2013, 2013.

Cubison, M. J., Ortega, A. M., Hayes, P. L., Farmer, D. K., Day, D., Lechner, M. J., Brune, W. H., Apel, E., Diskin, G. S., Fisher, J. A., Fuelberg, H. E., Hecobian, A., Knapp, D. J., Mikoviny, T., Riemer, D., Sachse, G. W., Sessions, W., Weber, R. J., Weinheimer, A. J., Wisthaler, A. and Jimenez, J. L.: Effects of aging on organic aerosol from open biomass burning

40 smoke in aircraft and laboratory studies, Atmos. Chem. Phys., 11(23), 12049–12064, doi:10.5194/acp-11-12049-2011, 2011.

Cusack, M., Alastuey, A., Pérez, N., Pey, J. and Querol, X.: Trends of particulate matter (PM 2.5) and chemical composition at a regional background site in the Western Mediterranean over the last nine years (2002-2010), Atmos. Chem. Phys., 12, 8341–8357, doi:10.5194/acp-12-8341-2012, 2012.

Delene, D. J. and Ogren, J. A.: Variability of aerosol optical properties at four North American surface monitoring sites, J. Atmos. Sci., 59, 1135–1149, 2002.

Draxler, R.R. and Rolph, G.D., 2015. HYSPLIT (HYbrid Single-Particle Lagrangian Integrated Trajectory) Model access via NOAA ARL READY Website (http://ready.arl.noaa.gov/HYSPLIT.php). NOAA Air Resources Laboratory, Silver Spring, MD.

Drinovec, L., Močnik, G., Zotter, P., Prévôt, A. S. H., Ruckstuhl, C., Coz, E., Rupakheti, M., Sciare, J., Müller, T., Wiedensohler, A. and Hansen, A. D. A.: The "dual-spot" Aethalometer: an improved measurement of aerosol black carbon with real-time loading compensation, Atmos. Meas. Tech., 8(5), 1965–1979, doi:10.5194/amt-8-1965-2015, 2015.

Escudero, M., Querol, X., Ávila, A. and Cuevas, E.: Origin of the exceedances of the European daily PM limit value in regional background areas of Spain, Atmos. Environ., 41, 4, 730-744, doi: 10.1016/j.atmosenv.2006.09.014, 2007a.

Escudero, M., Querol, X., Pey, J., Alastuey,A., Pérez, N., Ferreira, F., Alonso, S., Rodríguez, S. and Cuevas, E.: A methodology for the quantification of the net African dust load in air quality monitoring networks, Atmos. Environ., 41, 5516–5524, doi:10.1016/j.atmosenv.2007.04.047, 2007b.

Favez, O., El Haddad, I., Piot, C., Boréave, a., Abidi, E., Marchand, N., Jaffrezo, J. L., Besombes, J. L., Personnaz, M. B., Sciare, J., Wortham, H., George, C. and D'Anna, B.: Inter-comparison of source apportionment models for the estimation of wood burning aerosols during wintertime in an Alpine city (Grenoble, France), Atmos. Chem. Phys., 10, 5295–5314, doi:10.5194/acp-10-5295-2010, 2010.

Garcia-Hurtado, E., Pey, J., Borrás, E., Sánchez, P., Vera, T., Carratalá, A., Alastuey, A., Querol, X. and Vallejo, V. R.: Atmospheric PM and volatile organic compounds released from Mediterranean shrubland wildfires, Atmos. Environ., 89, 85–92, doi:10.1016/j.atmosenv.2014.02.016, 2014.

Harrison, R. M., Beddows, D. C. S., Jones, A. M., Calvo, A., Alves, C. and Pio, C.: An evaluation of some issues regarding the use of aethalometers to measure woodsmoke concentrations, Atmos. Environ., 80, 540–548, doi:10.1016/j.atmosenv.2013.08.026, 2013.

Herich, H., Hueglin, C. and Buchmann, B.: A 2.5 year's source apportionment study of black carbon from wood burning and fossil fuel combustion at urban and rural sites in Switzerland, Atmos. Meas. Tech., 4(7), 1409–1420, doi:10.5194/amt-4-1409-2011, 2011.

IPCC 2007: Climate Change 2007: The Physical Science Basis (Contribution ofWorking Group I to the Fourth Assessment Report of the Intergovernmental Panel on Climate Change), edited by: Solomon, S., Qin, D. Manning, M., Chen, Z., Marquis, M., Averyt, K. B., Tignor, M., and Miller, H. L., Cambridge Univ. Press, New York, USA, 131–217, 2007.

IPCC 2013: Climate Change 2013: The Physical Science Basis. Working Group I contribution to the IPCC fifth assessment report, Final Draft Underlying Scientific-Technical Assessment, Cambridge University Press, Cambridge, United Kingdom and New York, NY, USA, 2013.

Jacobson, M. Z.: Studying the effects of aerosols on vertical photolysis rate coefficient and temperature profiles over an urban airshed, J. Geophys. Res., 103(D9), 10593, doi:10.1029/98JD00287, 1998.

Jacobson, M. Z.: Global direct radiative forcing due to multicomponent anthropogenic and natural aerosols, J. Geophys. Res., 106(D2), 1551, doi:10.1029/2000JD900514, 2001.

Jiménez, P., Lelieveld, J. and Baldasano, J. M.: Multiscale modeling of air pollutants dynamics in the northwestern Mediterranean basin during a typical summertime episode, J. Geophys. Res., 111(D18), D18306, doi:10.1029/2005JD006516, 2006.

Jorba, O., Pandolfi, M., Spada, M., Baldasano, J. M., Pey, J., Alastuey, A., Arnold, D., Sicard, M., Artiñano, B., Revuelta, M. A. and Querol, X.: Overview of the meteorology and transport patterns during the DAURE field campaign and their impact to PM observations, Atmos. Environ., 77, 607–620, doi:10.1016/j.atmosenv.2013.05.040, 2013.

Kirchstetter, T. W., Novakov, T. and Hobbs, P. V.: Evidence that the spectral dependence of light absorption by aerosols is affected by organic carbon, J. Geophys. Res. D Atmos., 109, 1–12, doi:10.1029/2004JD004999, 2004.

Lack, D. a. and Cappa, C. D.: Impact of brown and clear carbon on light absorption enhancement, single scatter albedo and absorption wavelength dependence of black carbon, Atmos. Chem. Phys., 10(9), 4207–4220, doi:10.5194/acp-10-4207-2010, 2010.

Laj, P., Klausen, J., Bilde, M., Plaß-Duelmer, C., Pappalardo, G., Clerbaux, C., Baltensperger, U., Hjorth, J., Simpson, D., Reimann, S., Coheur, P. F., Richter, a., De Mazière, M., Rudich, Y., McFiggans, G., Torseth, K., Wiedensohler, A., Morin, S., Schulz, M., Allan, J. D., Attié, J. L., Barnes, I., Birmili, W., Cammas, J. P., Dommen, J., Dorn, H. P., Fowler, D., Fuzzi, S., Glasius, M., Granier, C., Hermann, M., Isaksen, I. S. A, Kinne, S., Koren, I., Madonna, F., Maione, M., Massling, A., Moehler, O., Mona, L., Monks, P. S., Müller, D., Müller, T., Orphal, J., Peuch, V. H., Stratmann, F., Tanré, D., Tyndall, G., Abo Riziq, a., Van Roozendael, M., Villani, P., Wehner, B., Wex, H. and Zardini, a. a.: Measuring atmospheric composition change, Atmos. Environ., 43, 5351–5414, doi:10.1016/j.atmosenv.2009.08.020, 2009.

Laskin, A., Laskin, J. and Nizkorodov, S. A.: Chemistry of Atmospheric Brown Carbon., Chem. Rev., 115(10), 4335–4382, doi:10.1021/cr5006167, 2015.

Lewis, K., Arnott, W. P., Moosmüller, H. and Wold, C. E.: Strong spectral variation of biomass smoke light absorption and single scattering albedo observed with a novel dual-wavelength photoacoustic instrument, J. Geophys. Res., 113(D16), D16203, doi:10.1029/2007JD009699, 2008.

Marcq, S., Laj, P., Roger, J. C., Villani, P., Sellegri, K., Bonasoni, P., Marinoni, A., Cristofanelli, P., Verza, G. P. and Bergin, M.: Aerosol optical properties and radiative forcing in the high Himalaya based on measurements at the Nepal Climate Observatory-Pyramid site (5079 m a.s.l.), Atmos. Chem. Phys., 10(13), 5859–5872, doi:10.5194/acp-10-5859-2010, 2010.

Mallet, M., Dubovik, O., Nabat, P., Dulac, F., Kahn, R., Sciare, J., Paronis, D., and Léon, J. F.: Absorption properties of Mediterranean aerosols obtained from multi-year ground-based remote sensing observations, Atmos. Chem. Phys., 13, 9195-9210, doi:10.5194/acp-13-9195-2013, 2013.

Millán, M. M., Salvador, R., Mantilla, E. and Kallos, G.: Photooxidant dynamics in the Mediterranean basin in summer: Results from European research projects, J. Geophys. Res., 102(D7), 8811, doi:10.1029/96JD03610, 1997.

Minguillón, M. C., Perron, N., Querol, X., Szidat, S., Fahrni, S. M., Alastuey, A., Jimenez, J. L., Mohr, C., Ortega, a. M., Day, D. A., Lanz, V. A., Wacker, L., Reche, C., Cusack, M., Amato, F., Kiss, G., Hoffer, A., Decesari, S., Moretti, F., Hillamo, R., Teinilä, K., Seco, R., Peñuelas, J., Metzger, a., Schallhart, S., Müller, M., Hansel, A., Burkhart, J. F., Baltensperger, U. and Prévót, a. S. H.: Fossil versus contemporary sources of fine elemental and organic carbonaceous particulate matter during the DAURE campaign in Northeast Spain, Atmos. Chem. Phys., 11(23), 12067–12084, doi:10.5194/acp-11-12067-2011, 2011.

Minguillón, M. C., Ripoll, A., Pérez, N., Prévôt, A. S. H., Canonaco, F., Querol, X. and Alastuey, A.: Chemical characterization of submicron regional background aerosols in the western Mediterranean using an Aerosol Chemical Speciation Monitor, Atmos. Chem. Phys., 15(11), 6379–6391, doi:10.5194/acp-15-6379-2015, 2015.

Mohr, C., DeCarlo, P. F., Heringa, M. F., Chirico, R., Slowik, J. G., Richter, R., Reche, C., Alastuey, A., Querol, X., Seco, R., Peñuelas, J., Jiménez, J. L., Crippa, M., Zimmermann, R., Baltensperger, U. and Prévôt, A. S. H.: Identification and quantification of organic aerosol from cooking and other sources in Barcelona using aerosol mass spectrometer data, Atmos. Chem. Phys., 12(4), 1649–1665, doi:10.5194/acp-12-1649-2012, 2012.

Moosmüller, H. and Chakrabarty, R. K.: Technical Note: Simple analytical relationships between Ångström coefficients of aerosol extinction, scattering, absorption, and single scattering albedo, Atmos. Chem. Phys., 11(20), 10677–10680, doi:10.5194/acp-11-10677-2011, 2011.

Müller, T., Henzing, J. S., de Leeuw, G., Wiedensohler, A., Alastuey, A., Angelov, H., Bizjak, M., Collaud Coen, M., Engström, J. E., Gruening, C., Hillamo, R., Hoffer, A., Imre, K., Ivanow, P., Jennings, G., Sun, J. Y., Kalivitis, N., Karlsson, H., Komppula, M., Laj, P., Li, S.-M., Lunder, C., Marinoni, A., Martins dos Santos, S., Moerman, M., Nowak, A., Ogren, J. A., Petzold, A., Pichon, J. M., Rodriquez, S., Sharma, S., Sheridan, P. J., Teinilä, K., Tuch, T., Viana, M., Virkkula, A., Weingartner, E., Wilhelm, R. and Wang, Y. Q.: Characterization and intercomparison of aerosol absorption photometers: result of two intercomparison workshops, Atmos. Meas. Tech., 4(2), 245–268, doi:10.5194/amt-4-245-2011, 2011a.

Müller, T., Laborde, M., Kassell, G. and Wiedensohler, A.: Design and performance of a three-wavelength LED-based total scatter and backscatter integrating nephelometer, Atmos. Meas. Tech., 4(6), 1291–1303, doi:10.5194/amt-4-1291-2011, 2011b.

Nickovic, S., Kallos, G., Papadopoulos, A. and Kakaliagou, O.: A model for prediction of desert dust cycle in the atmosphere, J. Geophys. Res., 106(D16), 18113, doi:10.1029/2000JD900794, 2001.

Ogren, J. A., Andrews, E., McComiskey, A., Sheridan, P., Jefferson, A., and Fiebig, M.: New insights into aerosol asymmetry parameter, in: Proceedings of the 16th ARM Science Team Meeting, Albuquerque, NM, USA, 2006.

Pandolfi, M., Cusack, M., Alastuey, a. and Querol, X.: Variability of aerosol optical properties in the Western Mediterranean Basin, Atmos. Chem. Phys., 11(15), 8189–8203, doi:10.5194/acp-11-8189-2011, 2011.

Pandolfi, M., Ripoll, A., Querol, X. and Alastuey, A.: Climatology of aerosol optical properties and black carbon mass absorption cross section at a remote high-altitude site in the western Mediterranean Basin, Atmos. Chem. Phys., 14(12), 6443–6460, doi:10.5194/acp-14-6443-2014, 2014a.

Pandolfi, M., Querol, X., Alastuey, A., Jimenez, J. L., Jorba, O., Day, D., Ortega, A., Cubison, M. J., Comerón, A., Sicard, M., Mohr, C., Prévôt, A. S. H., Minguillón, M. C., Pey, J., Baldasano, J. M., Burkhart, J. F., Seco, R., Peñuelas, J., van Drooge, B. L., Artiñano, B., Di Marco, C., Nemitz, E., Schallhart, S., Metzger, A., Hansel, A., Lorente, J., Ng, S., Jayne, J. and Szidat, S.: Effects of sources and meteorology on particulate matter in the Western Mediterranean Basin: An overview of the DAURE campaign, J. Geophys. Res. Atmos., 119(8), 4978–5010, doi:10.1002/2013JD021079, 2014b.

Pérez, C., Sicard, M., Jorba, O., Comerón, A. and Baldasano, J. M.: Summertime re-circulations of air pollutants over the north-eastern Iberian coast observed from systematic EARLINET lidar measurements in Barcelona, Atmos. Environ., 38, 3983–4000, doi:10.1016/j.atmosenv.2004.04.010, 2004.

Pérez, N., Pey, J., Castillo, S., Viana, M., Alastuey, A. and Querol, X.: Interpretation of the variability of levels of regional background aerosols in the Western Mediterranean, Sci. Total Environ., 407(1), 527–540, doi:10.1016/j.scitotenv.2008.09.006, 2008.

Petzold, A. and Schönlinner, M.: Multi-angle absorption photometry—a new method for the measurement of aerosol light absorption and atmospheric black carbon, J. Aerosol Sci., 35(4), 421–441, doi:10.1016/j.jaerosci.2003.09.005, 2004.

Petzold, A., Rasp, K., Weinzierl, B., Esselborn, M., Hamburguer, T., Dörnbrack, A., Kandler, K., Schütz, L., Knippertz, P., Fiebig, M. and Virkkula, A.: Saharan dust absorption and refractive index from aircraft-based observations during SAMUM 2006, Tellus B, 61(1), 118–130, doi:10.1111/j.1600-0889.2008.00383.x, 2009.

Petzold, A., Ogren, J. A., Fiebig, M., Laj, P., Li, S.-M., Baltensperger, U., Holzer-Popp, T., Kinne, S., Pappalardo, G., Sugimoto, N., Wehrli, C., Wiedensohler, A. and Zhang, X.-Y.: Recommendations for reporting "black carbon" measurements, Atmos. Chem. Phys., 13(16), 8365–8379, doi:10.5194/acp-13-8365-2013, 2013.

Pey, J., Pérez, N., Querol, X., Alastuey, A., Cusack, M. and Reche, C.: Intense winter atmospheric pollution episodes affecting the Western Mediterranean., Sci. Total Environ., 408(8), 1951–9, doi:10.1016/j.scitotenv.2010.01.052, 2010.

Pey, J., Querol, X., Alastuey, A., Forastiere, F. and Stafoggia, M.: African dust outbreaks over the Mediterranean Basin during 2001–2011: PM10 concentrations, phenomenology and trends, and its relation with synoptic and mesoscale meteorology, Atmos. Chem. Phys., 13(3), 1395–1410, doi:10.5194/acp-13-1395-2013, 2013a.

Pey, J., Pérez, N., Cortés, J., Alastuey, A. and Querol, X.: Chemical fingerprint and impact of shipping emissions over a western Mediterranean metropolis: primary and aged contributions., Sci. Total Environ., 463-464, 497–507, doi:10.1016/j.scitotenv.2013.06.061, 2013b.

Pope, C. A. and Dockery, D. W.: Health effects of fine particulate air pollution: lines that connect., J. Air Waste Manag. Assoc., 56(6), 709–42, 2006.

Querol, X., Pey, J., Pandolfi, M., Alastuey, a., Cusack, M., Pérez, N., Moreno, T., Viana, M., Mihalopoulos, N., Kallos, G. and Kleanthous, S.: African dust contributions to mean ambient PM10 mass-levels across the Mediterranean Basin, Atmos. Environ., 43, 4266–4277, doi:10.1016/j.atmosenv.2009.06.013, 2009.

Ramanathan, V. and Carmichael, G.: Global and regional climate changes due to black carbon, Nat. Geosci., 1(4), 221–227, doi:10.1038/ngeo156, 2008.

Reche, C., Viana, M., Amato, F., Alastuey, A., Moreno, T., Hillamo, R., Teinilä, K., Saarnio, K., Seco, R., Peñuelas, J., Mohr, C., Prévôt, A. S. H. and Querol, X.: Biomass burning contributions to urban aerosols in a coastal Mediterranean City, Sci. Total Environ., 427-428, 175–190, doi:10.1016/j.scitotenv.2012.04.012, 2012.

Ripoll, A., Pey, J., Minguillón, M. C., Pérez, N., Pandolfi, M., Querol, X. and Alastuey, A.: Three years of aerosol mass, black carbon and particle number concentrations at Montsec (southern Pyrenees, 1570 m a.s.l.), Atmos. Chem. Phys., 14, 4279–4295, doi:10.5194/acp-14-4279-2014, 2014.

Ripoll, A., Minguillón, M. C., Pey, J., Pérez, N., Querol, X. and Alastuey, A.: Joint analysis of continental and regional background environments in the western Mediterranean: PM1 and PM10 concentrations and composition, Atmos. Chem. Phys., 15(2), 1129–1145, doi:10.5194/acp-15-1129-2015, 2015b.

Rodríguez, S., Querol, X., Alastuey, A., Kallos, G. and Kakaliagou, O.: Saharan dust contributions to PM10 and TSP levels in Southern and Eastern Spain, Atmos. Environ., 35(2001), 2433–2447, doi:10.1016/S1352-2310(00)00496-9, 2001.

Rodríguez, S., Querol, X., Alastuey, A. and Plana, F.: Sources and processes affecting levels and composition of atmospheric aerosol in the western Mediterranean, J. Geophys. Res., 107(D24), 4777, doi:10.1029/2001JD001488, 2002.

Rodríguez, S., Querol, X., Alastuey, A., Viana, M.-M. and Mantilla, E.: Events Affecting Levels and Seasonal Evolution of Airborne Particulate Matter Concentrations in the Western Mediterranean, Environ. Sci. Technol., 37(2), 216–222, doi:10.1021/es020106p, 2003.

Rodríguez, S., Alastuey, A., Alonso-Pérez, S., Querol, X., Cuevas, E., Abreu-Afonso, J., Viana, M., Pérez, N., Pandolfi, M. and de la Rosa, J.: Transport of desert dust mixed with North African industrial pollutants in the subtropical Saharan Air Layer, Atmos. Chem. Phys., 11(13), 6663–6685, doi:10.5194/acp-11-6663-2011, 2011.

Rodríguez, S., Cuevas, E., Prospero, J. M., Alastuey, A., Querol, X., López-Solano, J., García, M. I., and Alonso-Pérez, S.: Modulation of Saharan dust export by the North African dipole, Atmos. Chem. Phys., 15, 7471-7486, doi:10.5194/acp-15-7471-2015, 2015.

Rolph, G.D., 2015. Real-time Environmental Applications and Display system (READY) Website (http://ready.arl.noaa.gov). NOAA Air Resources Laboratory, Silver Spring, MD.

Russell, P. B., Bergstrom, R. W., Shinozuka, Y., Clarke, A. D., DeCarlo, P. F., Jimenez, J. L., Livingston, J. M., Redemann, J., Dubovik, O., and Strawa, A.: Absorption Angstrom Exponent in AERONET and related data as an indicator of aerosol composition, Atmos. Chem. Phys., 10, 1155-1169, doi:10.5194/acp-10-1155-2010, 2010.

Sandradewi, J., Prévôt, A. S. H., Szidat, S., Perron, N., Alfarra, M. R., Lanz, V. A., Weingartner, E. and Baltensperger, U.: Using Aerosol Light Absorption Measurements for the Quantitative Determination of Wood Burning and Traffic Emission Contributions to Particulate Matter, Environ. Sci. Technol., 42(9), 3316–3323, doi:10.1021/es702253m, 2008b.

Schuster, G. L., Dubovik, O. and Holben, B. N.: Angstrom exponent and bimodal aerosol size distributions, J. Geophys. Res., 111(D7), D07207, doi:10.1029/2005JD006328, 2006.

Seco, R., J. Peñuelas, I. Filella, J. Llusia, S. Schallhart, A. Metzger, M. Müller, and A. Hansel: Volatile organic compounds in the western Mediterranean basin: Urban and rural winter measurements during the DAURE campaign, Atmos. Chem. Phys., 13, 4291–4306, doi:10.5194/acp-13-4291-2013.

Segura, S., Estellés, V., Titos, G., Lyamani, H., Utrillas, M. P., Zotter, P., Prévôt, A. S. H., Močnik, G., Alados-Arboledas, L., and Martínez-Lozano, J. A.: Determination and analysis of in situ spectral aerosol optical properties by a multi-instrumental approach, Atmos. Meas. Tech., 7, 2373-2387, doi:10.5194/amt-7-2373-2014, 2014.

Seinfeld, J. H., and S. N. Pandis (1998), Atmospheric Chemistry and Physics: From Air Pollution to Climate Change, 1326 pp., John Wiley, Hoboken, N. J.

Sokolik, I. N. and Toon, O. B.: Incorporation of mineralogical composition into models of the radiative properties of mineral aerosol from UV to IR wavelengths, J. Geophys. Res., 104(D8), 9423, doi:10.1029/1998JD200048, 1999.

Steinbrecher, R., Smiatek, G., Köble, R., Seufert, G., Theloke, J., Hauff, K., Ciccioli, P., Vautard, R. and Curci, G.: Intra- and inter-annual variability of VOC emissions from natural and semi-natural vegetation in Europe and neighbouring countries, Atmos. Environ., 43(7), 1380–1391, doi:10.1016/j.atmosenv.2008.09.072, 2009.

Twomey, S. A., Piepgrass, M. and Wolfe, T. L.: An assessment of the impact of pollution on global cloud albedo, Tellus B, 36B(5), 356–366, doi:10.1111/j.1600-0889.1984.tb00254.x, 1984.

Valenzuela, A., Olmo, F. J., Lyamani, H., Antón, M., Titos, G., Cazorla, A. and Alados-Arboledas, L.: Aerosol scattering and absorption Angström exponents as indicators of dust and dust-free days over Granada (Spain), Atmos. Res., 154, 1–13, doi:10.1016/j.atmosres.2014.10.015, 2015.

Viana, M., Reche, C., Amato, F., Alastuey, A., Querol, X., Moreno, T., Lucarelli, F., Nava, S., Calzolai, G., Chiari, M. and Rico, M.: Evidence of biomass burning aerosols in the Barcelona urban environment during winter time, Atmos. Environ., 72, 81–88, doi:10.1016/j.atmosenv.2013.02.031, 2013.

Weingartner, E., Saathoff, H., Schnaiter, M., Streit, N., Bitnar, B. and Baltensperger, U.: Absorption of light by soot particles: Determination of the absorption coefficient by means of aethalometers, J. Aerosol Sci., 34(10), 1445–1463, doi:10.1016/S0021-8502(03)00359-8, 2003.

Yang, M., Howell, S. G., Zhuang, J., and Huebert, B. J.: Attribution of aerosol light absorption to black carbon, brown carbon, and dust in China – interpretations of atmospheric measurements during EAST-AIRE, Atmos. Chem. Phys., 9, 2035-2050, doi:10.5194/acp-9-2035-2009, 2009.

Table 1. Extensive and intensive aerosol optical properties measured and derived, respectively, in this work.

Extensive optical properties				
Optical properties of PM$_{10}$ particles	symbol	λ [nm]	method	notes
Scattering	$\sigma_{spPM_{10}}^{\lambda}$	450, 525, 635	Nephelometer[AURORA 3000 ECOTECH Pty,Ltd, Knoxfield, Australia]	Measurements corrected for truncation and non-Lambertian illumination function of the light source as in Müller et al. (2011b)
Backscattering	$\sigma_{bspPM_{10}}^{\lambda}$			
Absorption	$\sigma_{apPM_{10}}^{\lambda}$	370, 470, 520, 590, 660, 880, 950	Aethalometers model AE-31 and AE-33[MAGEE Scientific]	AE-31 measurements corrected for filter loading as in Weingartner et al. (2003) and Collaud Coen et al. (2010)
Intensive optical properties				
Scattering Ångström exponent	SAE	450 to 635	$SAE = -Linear\ estimation$ $\left(\dfrac{Ln(\sigma_{spPM_{10}}^{\lambda_1} to\ \sigma_{spPM_{10}}^{\lambda_3})}{Ln(\lambda_1\ to\ \lambda_3)} \right)$	
Absorption Ångström exponent	AAE	370 to 950	$AAE = -Linear\ estimation$ $\left(\dfrac{Ln(\sigma_{apPM_{10}}^{\lambda_1} to\ \sigma_{apPM_{10}}^{\lambda_7})}{Ln(\lambda_1\ to\ \lambda_7)} \right)$	
Asymmetry parameter	g	450, 525, 635	$g(\lambda) = -7.14\left(\sigma_{bsp}^{\lambda}\big/\sigma_{sp}^{\lambda} \right)^3 + 7.46\left(\sigma_{bsp}^{\lambda}\big/\sigma_{sp}^{\lambda} \right)^2 - 3.96\left(\sigma_{bsp}^{\lambda}\big/\sigma_{sp}^{\lambda} \right) + 0.9893$	The nephelometer measures hemispheric backscattering [-90º - + 90º]
Single scattering albedo	SSA	370, 470, 520, 590, 660, 880, 950	$SSA(\lambda) = \dfrac{\sigma_{sp}^{\lambda}}{\sigma_{sp}^{\lambda} + \sigma_{ap}^{\lambda}}$	In order to estimate SSA at 7 λ, the scattering was calculated at 7 λ using the measured SAE.

| Single scattering albedo Ångström exponent | $SSAAE$ | 370 to 950 | $SSAAE = -Linear\ estimation$ $\left(\dfrac{Ln\left(SSA_{PM_{10}}^{\lambda_1}\ to\ SSA_{PM_{10}}^{\lambda_7}\right)}{Ln(\lambda_1\ to\ \lambda_7)}\right)$ | |

Table 2. C_1, C_2 and C_3 obtained by MLR on the Aethalometer model for different AAE_{bb} (1.8, 2, 2.2) keeping AAE_{ff}=1, and varying AAE_{ff} (0.9, 1.1) keeping AAE_{bb}=2 on hourly base at MSY.

Hourly data (5456)	AAE_{ff}=1		
	AAE_{bb}=1.8	AAE_{bb}=2	AAE_{bb}=2.2
C_1 (g m^{-2})	1.05153 ± 0.01004		
C_2 (g m^{-2})	0.27998 ± 0.00314	0.26021 ± 0.00354	0.24384 ± 0.00393
C_3 (µg m^{-3})	0.31433 ± 0.04051		
	AAE_{bb}=2		
	AAE_{ff}=0.9	AAE_{ff}=1.1	
C_1 (g m^{-2})	1.01342 ± 0.01063	1.09341 ± 0.00959	
C_2 (g m^{-2})	0.26021 ± 0.00354		
C_3 (µg m^{-3})	0.31433 ± 0.04051		

Table 3. Squared Pearson (R^2) and slope (F) of the scatterplot between OM_{bb} and BBOA and between OM_{ff} and HOA, for different values of AAE_{bb} (1.6, 1.8, 2, 2.2) keeping AAE_{ff}=1 at MSY (hourly base).

		AAE_{ff}=1			
	AAE_{bb}	1.6	1.8	2	2.2
OM_{bb} vs. BBOA	R²	0.436	0.423	0.429	0.426
	F	2.160	1.440	1.274	1.064
OM_{ff} vs. HOA	R²	0.426	0.525	0.600	0.631
	F	4.002	4.240	4.377	4.467

Figure captions

Figure 1. (a) Location of Montsec (MSA; remote-mountaintop site) and Montseny (MSY; regional background) measurement sites. **(b)** Topographic profile of MSA and MSY area.

Figure 2. Ångström matrix (scatterplot of AAE vs. SAE weighted by air mass origin) at **(a)** MSY and **(d)** MSA. Ångström matrix (scatterplot of AAE vs. SAE weighted by levels of %PM$_{1-10}$ in PM$_{10}$) at **(b)** MSY and **(e)** MSA. Ångström-Asymmetry parameter matrix (scatterplot of AAE vs. g weighted by levels of %PM$_{1-10}$ in PM$_{10}$) at **(c)** MSY and **(f)** MSA. (On hourly base).

Figure 3. Relationship between SSAAE and the relative contribution (%) of: **(a)** mineral dust to PM$_{10}$ at MSY and **(b)** PM$_{1-10}$ to PM$_{10}$ at MSA. Case studies discussed in the text show hourly SAE, AAE and SSAAE calculated for MSY during the periods **(c)** 28/06/2012 and **(d)** 15/10/2013-09/11/2013. Yellow and blue rectangles in Fig. 3d indicate the occurrence of SDE and precipitation respectively.

Figure 4. Scatterplot by bins between OM$_{ff}$ and HOA, and between OM$_{bb}$ and BBOA for AAE$_{bb}$=2 and AAE$_{ff}$=1 at MSY (on hourly base).

Figure 5. Scatterplot between BC$_{ff}$ and NO$_2$ for winter season (from November to February,) during the period 2012–2014 at MSY (daily base).

Figure 6. Daily cycle of: **(a)** AAE at MSY and MSA, **(b)** measured OM and simulated OM as the sum of OM$_{ff}$ and OM$_{bb}$ contributions at MSY, measured BC and simulated BC as the sum of BC$_{ff}$ and BC$_{bb}$ contributions at **(c)** MSY and **(d)** MSA. Annual cycle of: **(e)** AAE at MSY and MSA, **(f)** measured OM and simulated OM as the sum of OM$_{ff}$ and OM$_{bb}$ contributions at MSY, measured BC and simulated BC as the sum of BC$_{ff}$ and BC$_{bb}$ contributions at **(g)** MSY and **(h)** MSA. The study period ranges between 14/06/2012-09/07/2013 for OM contributions and between 12/06/2012-31/12/2014 for BC contributions, depending on the availability of BC and OM experimental measurements, respectively. Averages were calculated from hourly base.

Figure 7. Scatterplot by bins between AAE and %BC$_{bb}$ at MSY and MSA. Error bars are one standard deviation of the averages calculated from daily values.

Figure 8. Daily cycle of: **(a)** AAE, **(b)** Measured OM and simulated OM as the sum of OM$_{ff}$ and OM$_{bb}$ contributions, **(c)** Measured BC and simulated BC as the sum of BC$_{ff}$ and BC$_{bb}$ contributions, during a wildfire episode (23 July 2012) at MSY.
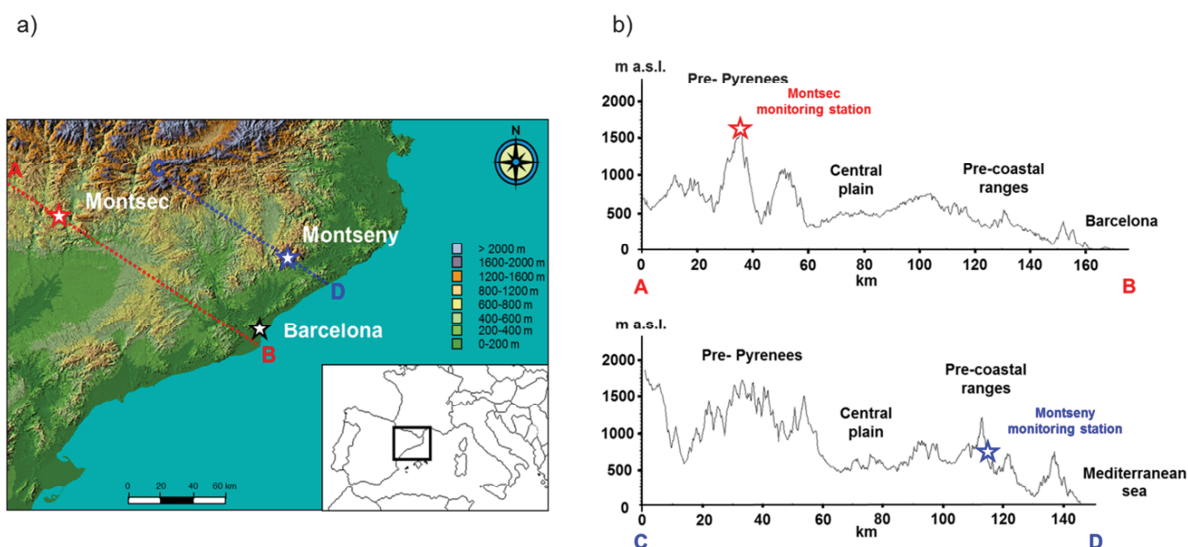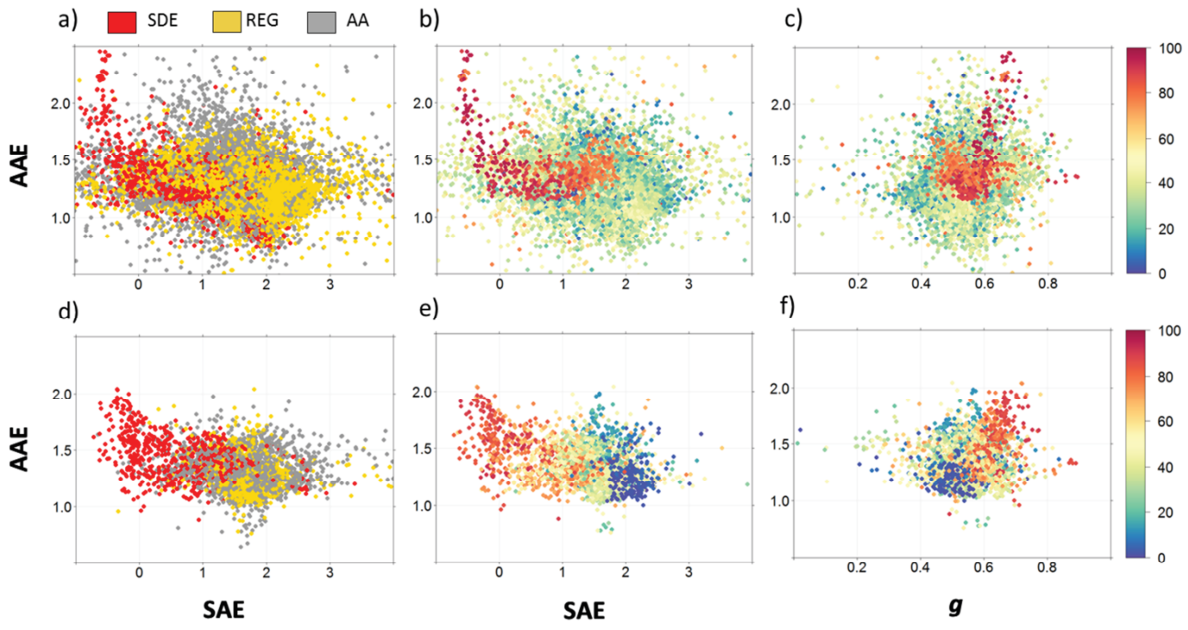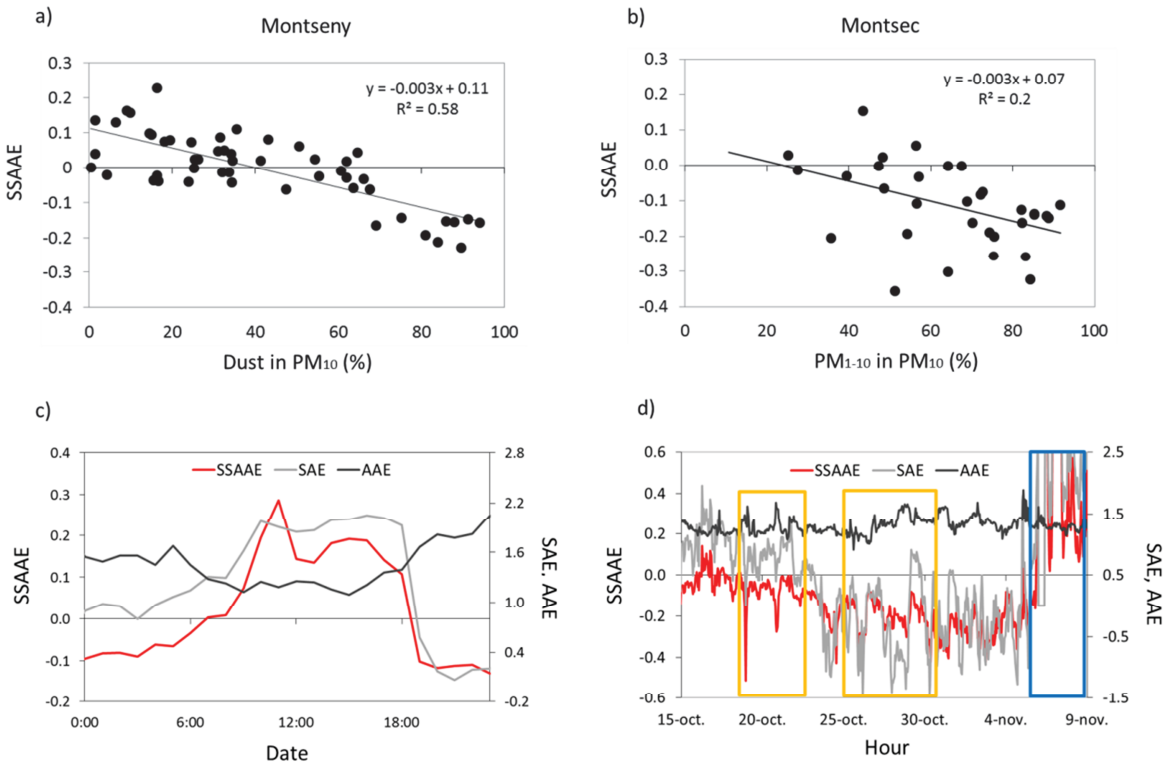
Figure 1

Figure 2

a) Montseny

$y = -0.003x + 0.11$
$R^2 = 0.58$

b) Montsec

$y = -0.003x + 0.07$
$R^2 = 0.2$

c)
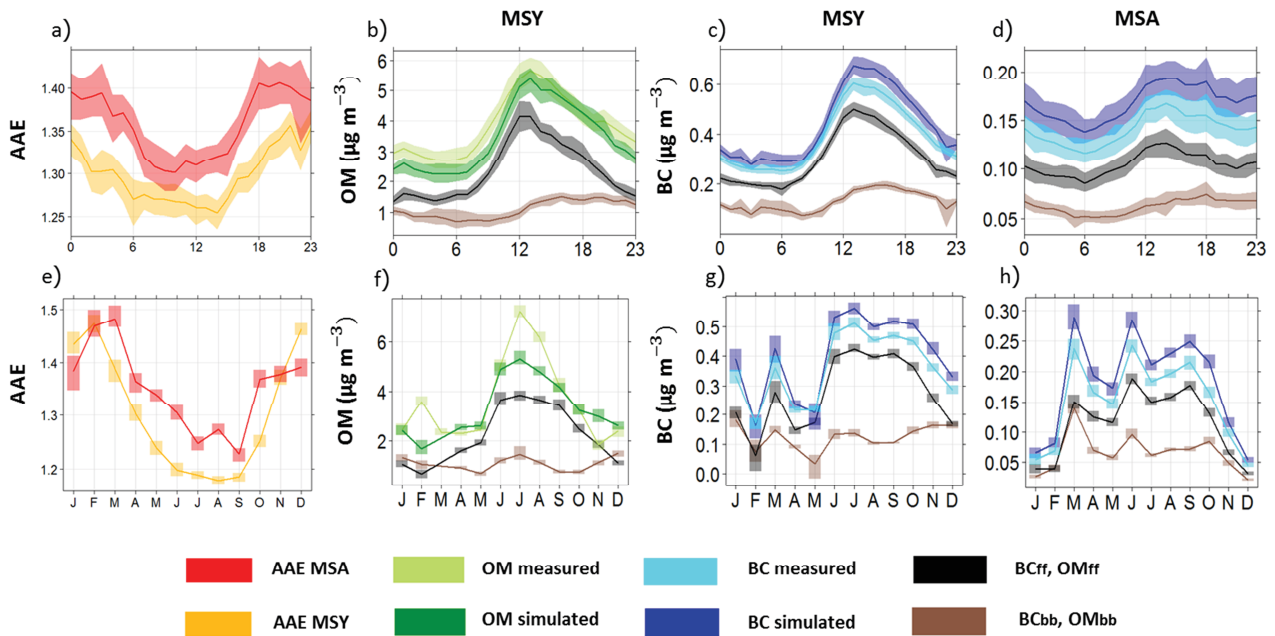
d)
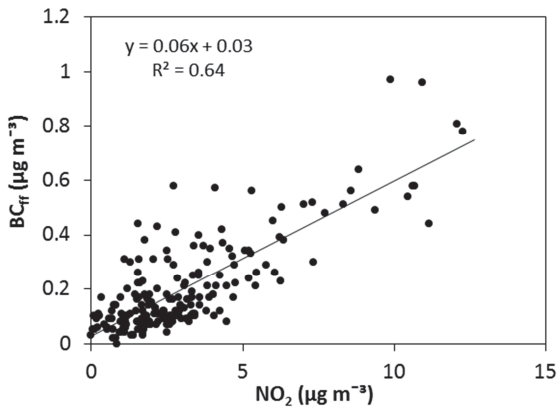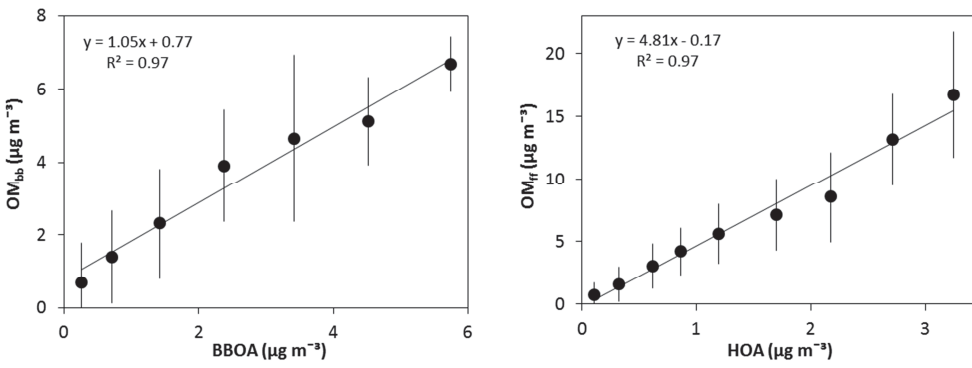
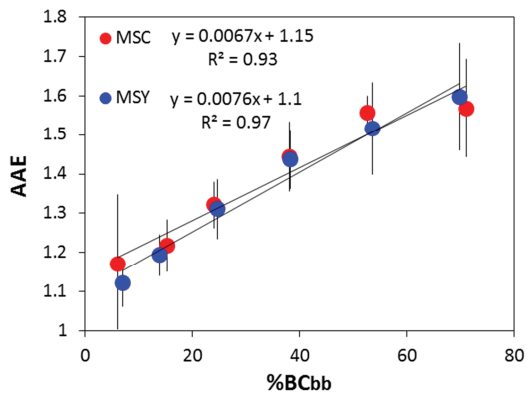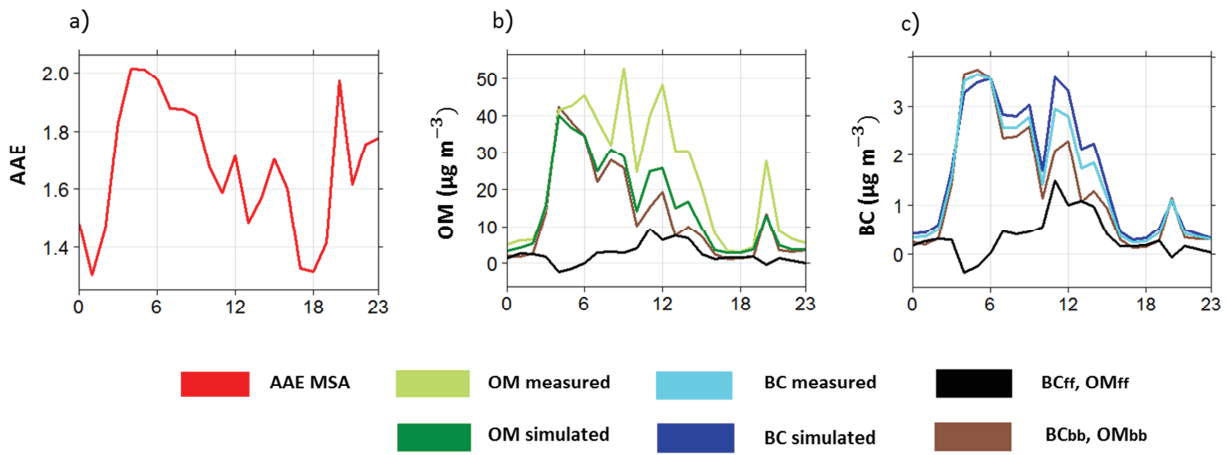**Figure 3**

Figure 4

5 **Figure 5**

Figure 6

Figure 7

Figure 8

Supplementary material of "Detection of Saharan dust and biomass burning events using near real-time intensive aerosol optical properties in the northwestern Mediterranean"

5 **Table S1.** List of acronyms

| Acronym	Definition
AA	Atlantic advections
AAE_{bb}	Fossil fuel absorption Ångström exponent
AAE_{ff}	Biomass burning absorption Ångström exponent
BB	Biomass burning
BBOA	Biomass burning organic aerosol
BC	Equivalent black carbon
BC_{ff}	Equivalent black carbon from fossil fuel source
BC_{bb}	Equivalent black carbon from biomass burning source
FF	Fossil fuel
g	Asymmetry parameter
HOA	Hydrocarbon-like organic aerosol
MSA	Montsec
MSY	Montseny
OM	Organic matter
OM_{bb}	Organic matter from biomass burning source
OM_{ff}	Organic matter from fossil fuel source
PBL	Planetary boundary layer
REG	Regional atmospheric episodes
SAE	Scattering Ångström exponent
SDE	Saharan dust event
SOA	Secondary organic aerosol
SSA	Single scattering albedo
SSAAE	Single scattering albedo Ångström exponent
WMB	Western Mediterranean Basin

Table S2~~1~~. Statistics from the hourly averages of the considered aerosol parameters for the period under study at MSY (~~a~~above) and MSA (below~~b~~) sites.

MSY	λ	Counts	Mean	SD	Median	Min	Max	Skewness	Percentiles				
									5	25	50	75	95
σ_{sp}	635	28443	30.05	27.67	23.53	-0.50	596.55	3.12	3.01	11.64	23.53	40.06	79.46
	525	28522	38.41	34.03	30.26	-0.50	539.71	2.52	4.27	14.98	30.26	51.72	100.42
	450	28540	47.26	41.29	37.35	-0.49	513.67	2.36	5.14	18.29	37.35	64.34	122.67
σ_{bsp}	635	25894	4.21	3.38	3.63	-0.50	60.56	2.12	0.26	1.77	3.63	5.87	10.06
	525	25974	4.67	3.76	4.01	-0.50	107.08	2.82	0.40	1.99	4.01	6.47	11.14
	450	25951	5.46	4.23	4.70	-0.50	58.86	2.08	0.57	2.40	4.70	7.51	12.86
g	635	23963	0.54	0.10	0.54	-0.97	0.97	-3.34	0.40	0.50	0.54	0.59	0.67
	525	24503	0.59	0.06	0.59	-0.46	0.90	-1.39	0.49	0.56	0.59	0.62	0.68
	450	25038	0.60	0.07	0.61	-0.94	0.88	-2.30	0.49	0.58	0.61	0.64	0.68
σ_{ap}	470	21580	7.66	6.50	6.04	-0.25	94.05	2.48	1.06	3.12	6.04	10.35	19.37
	880	21567	3.51	2.99	2.73	-0.21	31.43	2.10	0.44	1.37	2.73	4.81	9.02
SAE	450-635	27959	1.38	0.79	1.42	-2.45	5.98	0.14	0.06	1.01	1.42	1.76	2.48
AAE	370-950	21390	1.30	0.30	1.27	-1.86	5.84	0.69	0.91	1.14	1.27	1.44	1.75
SSA	470	13585	0.83	0.07	0.84	0.12	0.98	-1.69	0.70	0.80	0.84	0.88	0.91
	880	13575	0.80	0.12	0.83	0.05	1.00	-1.71	0.57	0.75	0.83	0.89	0.95
PM_{10}	-	35354	16.23	11.08	14.15	0.15	236.51	2.24	3.49	8.14	14.15	22.01	35.22

10

15

| MSA	λ	Counts	Mean	SD	Median	Min	Max	Skewness	Percentiles				
									5	25	50	75	95
σ_{sp}	635	21708	16.73	19.28	9.37	-0.50	307.33	2.05	0.22	2.77	9.37	25.19	54.79
	525	21790	22.12	25.09	12.44	-0.50	277.46	1.85	0.40	3.54	12.44	33.46	71.78
	450	21792	28.11	31.50	16.06	-0.50	376.38	1.80	0.59	4.53	16.06	42.70	91.38
σ_{bsp}	635	21728	2.29	2.51	1.38	-0.50	30.59	1.52	-0.13	0.35	1.38	3.68	7.14
	525	21757	2.69	2.91	1.60	-0.50	36.04	1.45	-0.09	0.41	1.60	4.30	8.36
	450	21542	3.19	3.43	1.94	-0.50	42.44	1.42	-0.10	0.46	1.94	5.16	9.82
g	635	18287	0.52	0.17	0.54	-1.00	0.94	-3.10	0.25	0.48	0.54	0.60	0.71
	525	18657	0.57	0.14	0.59	-1.00	0.94	-3.53	0.35	0.54	0.59	0.63	0.73
	450	18644	0.60	0.14	0.62	-1.00	0.94	-3.63	0.38	0.57	0.62	0.66	0.77
σ_{ap}	470	9913	3.57	3.95	2.03	-0.24	70.52	2.53	0.13	0.65	2.03	5.64	10.50
	880	9915	1.59	1.71	0.89	-0.16	23.03	1.79	0.06	0.29	0.89	2.57	4.81
SAE	450-635	20189	1.58	0.83	1.64	-1.95	6.00	-0.04	0.08	1.24	1.64	1.95	2.82
AAE	370-950	9625	1.36	0.27	1.32	-0.90	4.80	2.02	1.05	1.21	1.32	1.47	1.76
SSA	470	7146	0.85	0.08	0.87	0.21	1.00	-2.16	0.69	0.82	0.87	0.90	0.93
	880	7134	0.82	0.13	0.85	0.04	1.00	-2.29	0.57	0.79	0.85	0.89	0.95
PM_{10}	-	18782	11.32	9.93	8.46	0.10	153.62	2.60	1.36	4.84	8.46	15.54	29.51
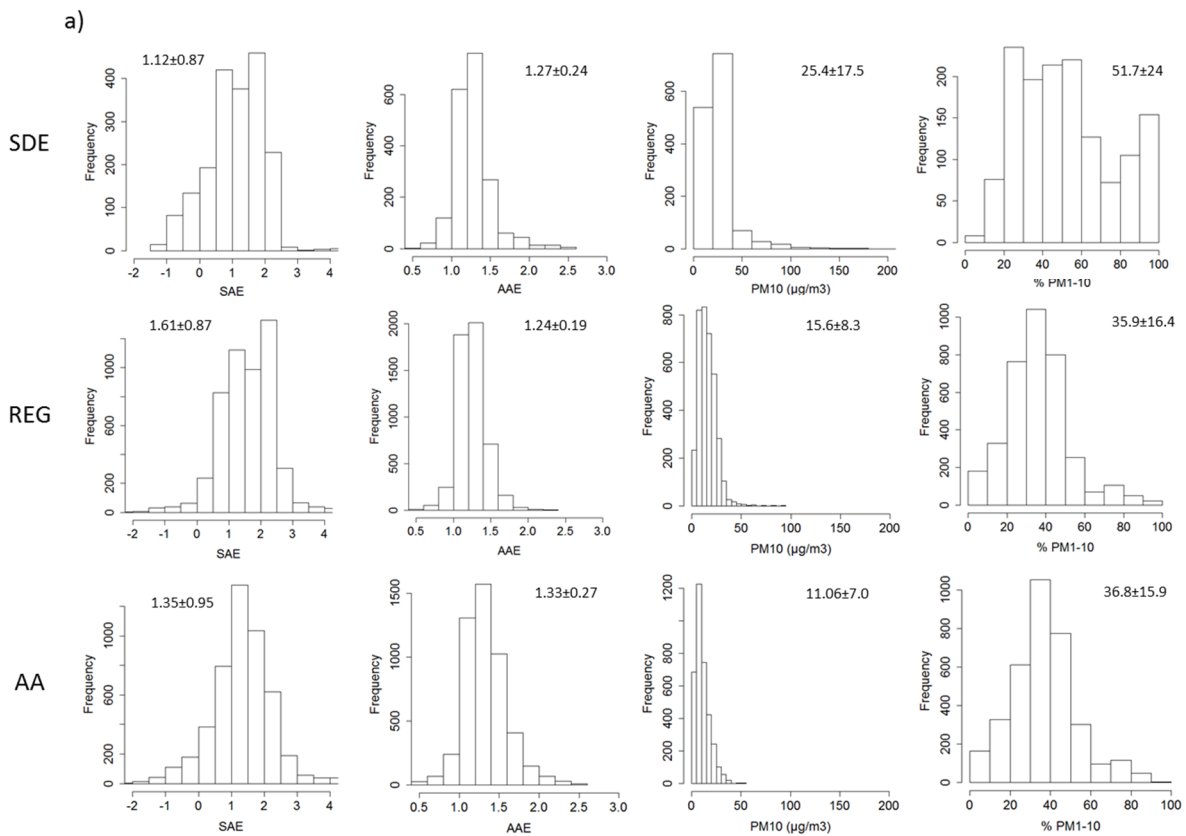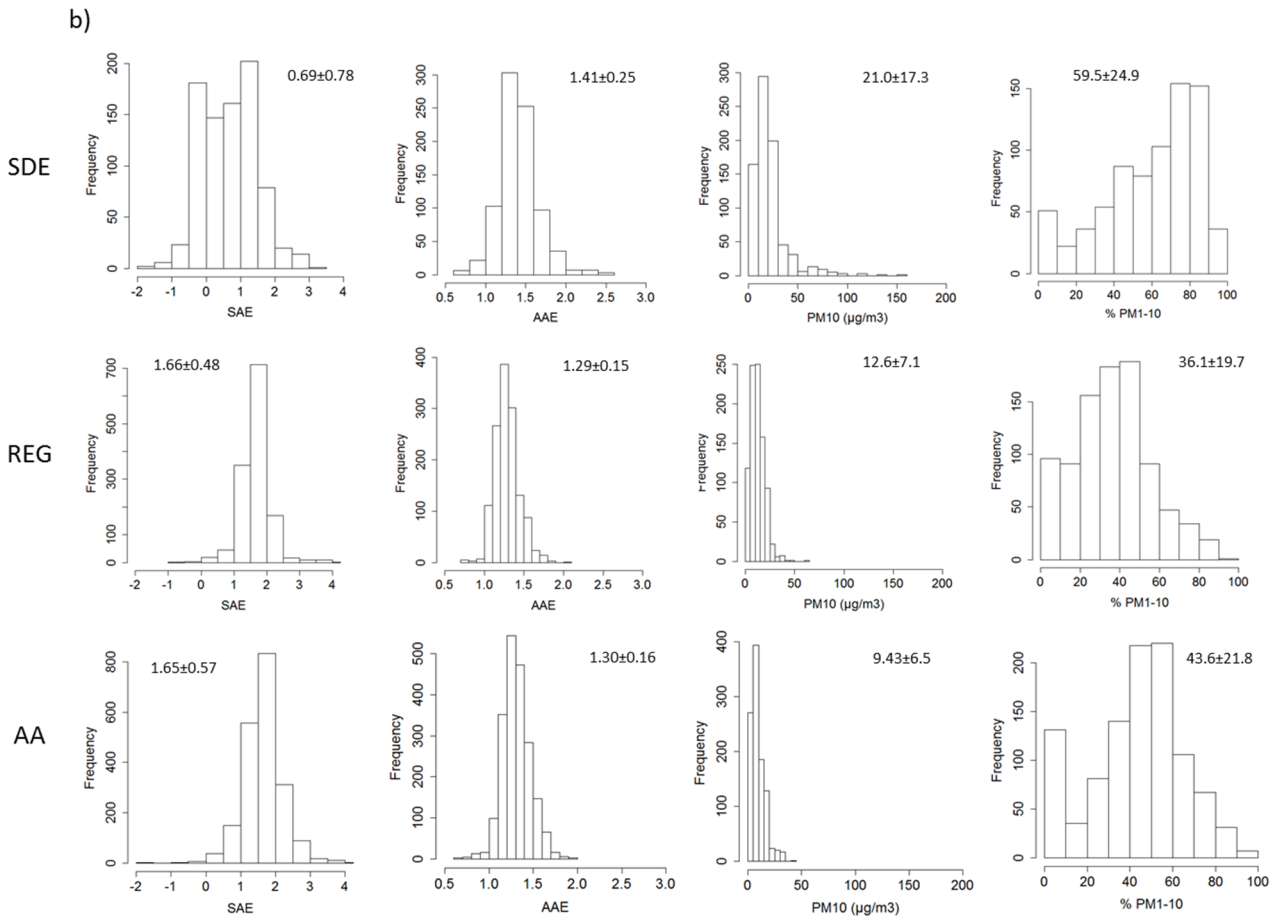
a)

Figure S1. Frequency distribution, average and standard deviation of SAE, AAE, PM$_{10}$ and %PM$_{1-10}$ in PM$_{10}$ parameters for the three atmospheric scenarios (SDE, REG, AA) displayed in the Ångström matrix at (a) MSY and (b) MSA.
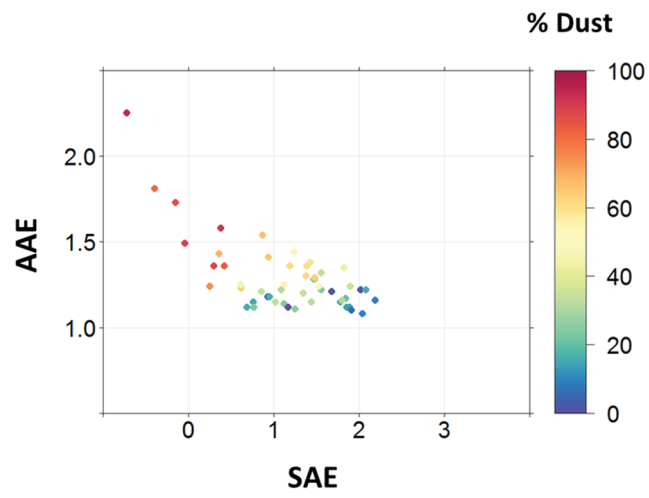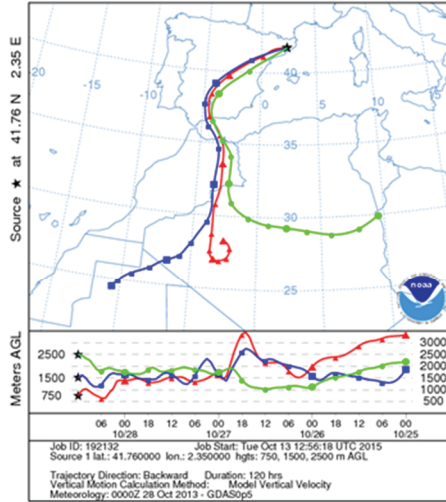
40   **Figure S2~~1~~.** Ångström matrix (AAE vs. SAE weighted by % dust in PM_{10}) during Saharan dust events at MSY (daily base).
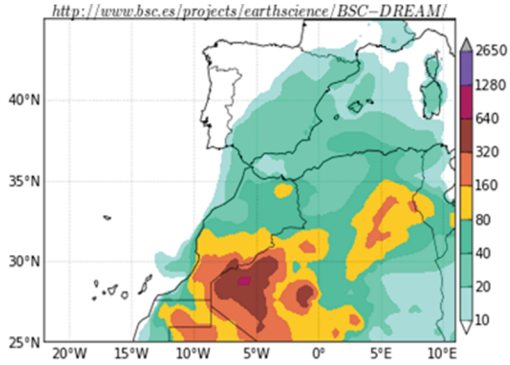
a)

NOAA HYSPLIT MODEL
Backward trajectories ending at 1200 UTC 01 Nov 13
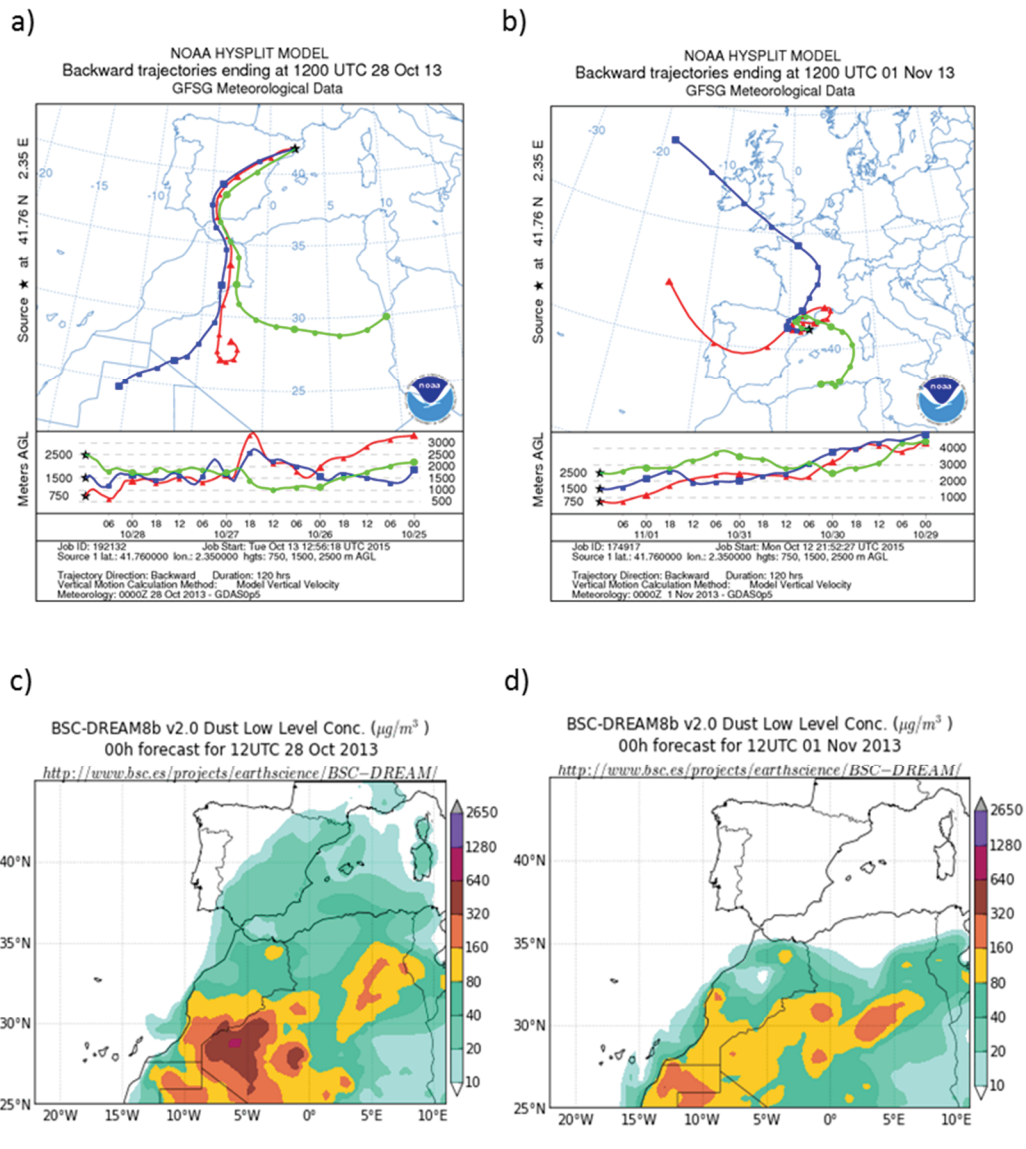GFSG Meteorological Data
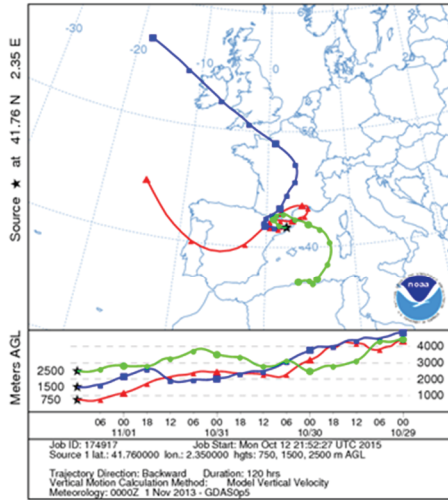
b)

NOAA HYSPLIT MODEL
Backward trajectories ending at 1200 UTC 28 Oct 13
GFSG Meteorological Data

c)

BSC-DREAM8b v2.0 Dust Low Level Conc. ($\mu g/m^3$)
00h forecast for 12UTC 28 Oct 2013
http://www.bsc.es/projects/earthscience/BSC-DREAM/

Figure S32. Backward trajectories corresponding to (a) the Saharan dust event (28/10/2013) and (b) the regional episode (01/11/2013) atmospheric scenarios at MSY. Dust surface concentration at MSY from the Dream model corresponding to (c) the Saharan dust event (28/10/2013) and (d) the regional episode (01/11/2013).
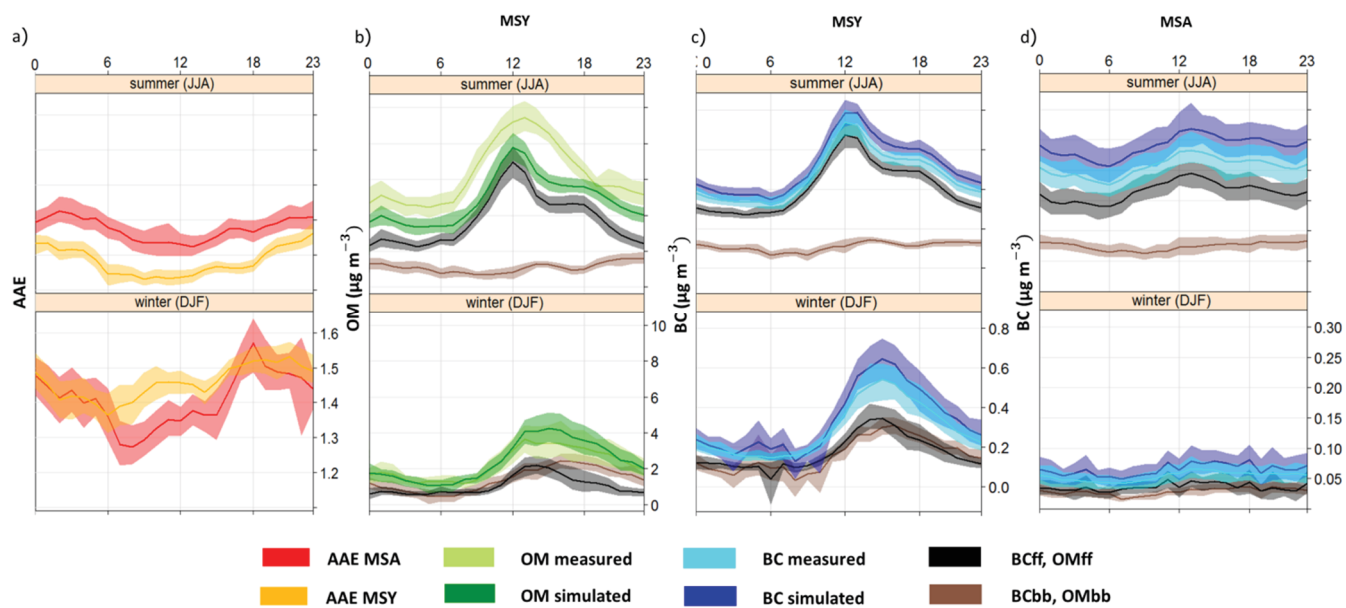
Figure S43. Summer and winter daily cycles of: (a) AAE at MSY and MSA, (b) measured OM and simulated OM as the sum of OMff and OMbb contributions at MSY, measured BC and simulated BC as the sum of BCff and BCbb contributions at (c) MSY and (d) MSA. Averages were calculated from hourly base.